Metal Nanoparticle Induced Enhancement of Light Absorption in Thin-film PV Cells

A Thesis Submitted to the Academic Faculty in Partial Fulfillment of the Requirements for the Degree of

BACHELOR OF SCIENCE IN ELECTRICAL AND ELECTRONIC ENGINEERING

Riyasat Ohib
Samin Yeasar
Sayem Ali

Department of Electrical and Electronic Engineering

Islamic University of Technology (IUT)
Gazipur, Bangladesh

November 2016

Declaration of Candidate

It is hereby declared that this thesis or any part of it has not been submitted elsewhere for the award of any Degree.

Supervised by

_____

Dr. Md. Ruhul Amin
Professor, Department of Electrical and Electronic Engineering,
Islamic University of Technology (IUT),
Boardbazar, Gazipur-1704.
Date:

Submitted by

_____

Riyasat Ohib
Student ID: 122429
Academic Year: 2013-2016
Date:

_____

Samin Yeasar
Student ID: 122454
Academic Year: 2013-2016
Date:

_____

Sayem Ali
Student ID: 122428
Academic Year: 2013-2016
Date:

Table of Contents

List of Figures

List of Tables

Acknowledgements

We would like convey our utmost gratitude to our thesis supervisor, Prof. Dr. Md. Ruhul Amin, for his continuous guidance and motivation in completing our thesis. Without his depth of knowledge and ideas our thesis work would be profoundly lacking. We would also like to thank Rakibul Islam Sagor, lecturer of the department of EEE, for his constant technical help with the simulation software (COMSOL), writing our research paper, building our thesis defense and many other things. His meticulous supervision and attention to details truly made this arduous task lot easier for us.

Abstract

The aim of this thesis is to investigate the utilization of plasmonic metal nanostructures for efficiency enhancement of thin-film solar cells. This efficiency enhancement strategy exploits the strong near-field enhancement and highly efficient light scattering that originates from localized surface plasmon resonances (LSPRs) excited in metal nanostructures and leads to an increased absorption in the solar cell active layer. In the first part of this thesis, the near-field enhancement is explained with rigorous theoretical details and how the electromagnetic characteristics alters significantly if a nanoparticle interacts with an incoming field. We have simulated in COMSOL the incoming electric and magnetic field pattern for a single dielectric particle. We have also shown the far-field radiation pattern and scattering characteristics. We have also demonstrated the enhanced resonant electric field (Hot Spot) and wavelength for peak electric field between 2 nanoparticles in close proximity. Later on, we have constructed models where we chose different metal nanoparticles (Al, Cu, Ag, Au) covered by thin-film absorber layer (GaAs, CdTe). We have measured the enhanced magnitude of absorption and scattering in presence of each of these nanoparticles which boosts the efficiency of an otherwise lacking thin-film absorber without the implementation of nanoparticles. Also we have demonstrated how varying the size of the nanoparticles impacted on the absorption enhancement. We have also delved into the recently emerging organic solar cell technology, very particularly, the Perovskite solar cell. Introducing nanoparticles into the Perovskite absorber layer results in higher absorption and scattering. We have measured the absorption enhancement in presence of different noble metal NPs (Al, Cu, Ag, Au). Also we have demonstrated the effect of the radius of the each of the metal NPs into absorption enhancement. Due to this absorption enhancement, the plasmonic nanostructured cell exhibits an enhanced power conversion efficiency compared to an optimized, high performance organic solar cell.

Chapter 1

Introduction

1.1 Motivation

One of the great challenges facing society today is the supply of low-cost, environmentally friendly energy sources that can meet the growing demands of an expanding population. As pointed out in reference [1] Photovoltaic power has the potential to meet these needs, since the amount of radiation striking the earth's surface is 1.76 x10^5 terawatts (TW) and current world usage is estimated at 15 TW. With respect to other renewable and nonrenewable energy resources, however, the cost of photovoltaic modules continues to be high, and cost per Watt remains the driving force behind much of photovoltaic research.

Concurrently, nanophotonics has emerged as a widespread area of research, with focus on both fundamentals of light control at the nanoscale and applications to devices. Subwavelength nanostructures enable the manipulation and molding of light in nanoscale dimensions. By controlling and designing the complex dielectric function and nanoscale geometry, the coupling of light into specific active materials can be controlled, and macroscale properties such as reflection, transmission, and absorption can be tuned. Applying the methods of nanophotonics to solar cells allows for the possibility of shrinking the absorbing layers while maintaining high levels of absorption, which enables higher efficiency, low cost, stable photovoltaic devices.

1.2 Objective

About 60% if the energy radiated from the sun reaches the Earth's surface; even if 0.1% of the energy could be converted at an efficiency of 10%, it would be four times larger than the total world's electricity generating capacity which is about 5000 GW. Among the various conversion systems, solar photovoltaics (SPV) systems is the most popular direct energy conversion system that converts solar energy in the visible spectrum (43% of the total radiated energy) directly to electricity. Conventionally, photovoltaics absorber must have 'optically thick' to allow near-complete light absorption and photocarrier current collection. A typical wafer-based crystalline solar cells have a much larger thickness of typically 180-300 um. But high-efficiency solar cell must have minority carrier diffusion lengths several times the material thickness for all photocarrier to be collected a requirement that is most easily met for thin cells, plus it reduces material cost. In an effort to reduce the wafer thickness to decrease carrier diffusion length and material all the while keeping the wafer optically thick, our objective is to somehow increase the incident light intensity. That is where the nanoparticles come in handy as they show enhanced radiation pattern and can manipulate light in subwavelength level. As noble metal nanoparticle exhibits localized surface plasmon resonances, their implementation can increase efficiency. Moreover, we must provide designs and simulations which would prove the viability of their impact in efficiency of conventional thin-film solar cells.

1.3 Solar Cell Overview

Solar photovoltaic cells are made from semiconductors, they are quantum devices and their efficiency largely depends on the bandgap. It can convert solar radiation with frequencies less than the bandgap of the cell materials. The efficiency is about 30%. Solar cell technology development can be broadly classified by the material composition of the active layer. Historically, crystalline Si has been the dominant semiconductor material for photovoltaics, although thin-film solar cells are gaining an increasing market share. Cited in [2], for Si approximately 50% of the total cost is due to the cost of the materials themselves, with the remainder due to cell production and module fabrication. While Si has many advantages as a material, including abundance and manufacturing experience, it is a relatively weak absorber, requiring 200 - 300 um of semiconductor material to fully absorb the incident sunlight. This Si must be high quality and defect free so that the generated carriers are not lost before collection. Study in reference [3] suggests that alternative thin-film photovoltaic cells with thicknesses of several microns have been developed with lower processing costs, but also lower efficiencies. For thin-film solar cells large fraction of the solar spectrum (600-1100 um) is poorly absorbed. Also in reference [4,5], it is found that the main thin-film solar technologies at present are Cadmium Telluride (CdTe), Gallium Arsenide (GaAs), Copper Indium Gallium Selenide (CIGS), and thin-film Si, with the record efficiency of these devices at 19.9% (CIGS).

1.4 Solar Cell Fundamentals

The purpose of a solar cell is to convert incident sunlight to electrical power. When an incident photon hits a solar cell, there are several possible outcomes. It can simply reflect of the surface. As shown in Fig. 1.1, if the energy of the photon is lower than the bandgap of the semiconductor (hf < Eg), it can pass through the semiconductor without absorption. If the energy of the photon is higher than the bandgap of the semiconductor (hf > Eg) then it can be absorbed by the semiconductor, exciting an electron from the valance band to the conduction band and generating an electron-hole pair (as well as heat, depending on the semiconductor).

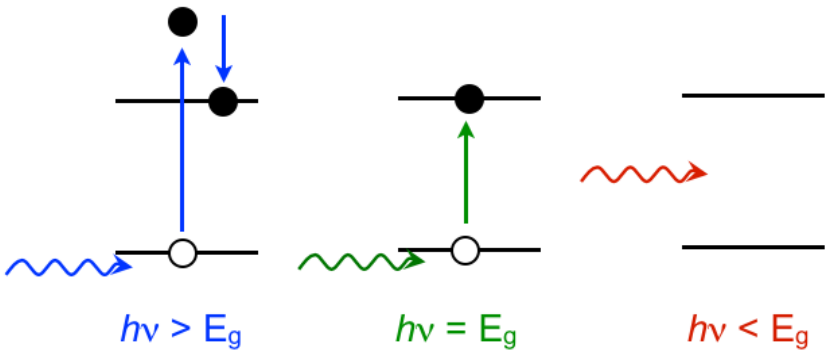

Figure 1.1: Photon energy compared to bandgap of a semiconductor.

Solar cells typically include other layers besides the semiconductor, such as contact layers and window layers, which can also parasitically absorb incident sunlight. Efficient solar cells minimize the losses due to reflection and absorption in other materials to maximize absorption in the semiconductor. After an electron-hole pair is generated, the electron and hole must be separated and driven to collection at separate electrodes. The charge separation occurs at a location of higher electric field. In a standard p-n junction, this occurs by diffusion. The charge carriers diffuse to a p-n junction within the semiconductor and are separated by the electric field at a junction. In a p-i-n device architecture, as commonly used in a-Si:H cells, there is an electric field across the entire device which drives the carriers to separation by drift rather than diffusion. Once the carriers are separated they are collected by the electrodes, generating current. Not all photogenerated electrons and holes are collected; other processes such as recombination can prevent the carriers from reaching the electrodes. Efficient solar cells therefore need to absorb the solar spectrum with minimal losses to reflection or materials other than the semiconductor, and efficiently separate the carriers and collect them externally. This thesis deals primarily with the first challenge: we design nanostructures to absorb light in small volumes of material, and integrate them into photovoltaic devices to study the effects. Carrier collection is not explicitly addressed, but the ultrathin semiconductor volumes used here may improve collection efficiencies as well. There are two primary challenges to designing solar cells with high absorption: first, the cell must absorb over the entire solar spectrum where the semiconductor is active, which is quite broad, and second the absorption must be high at all angles of incident sunlight. Naturally the angle of incidence changes throughout the day and season, as depicted in Fig. 1.2(a), but the angle will also vary due to diffuse scattering from clouds and other objects (Fig. 1.2(b)). While tracking devices can be used to optimize the angle of incidence of the sun, it is nevertheless important for solar panels to operate well at a wide range of incident angles.

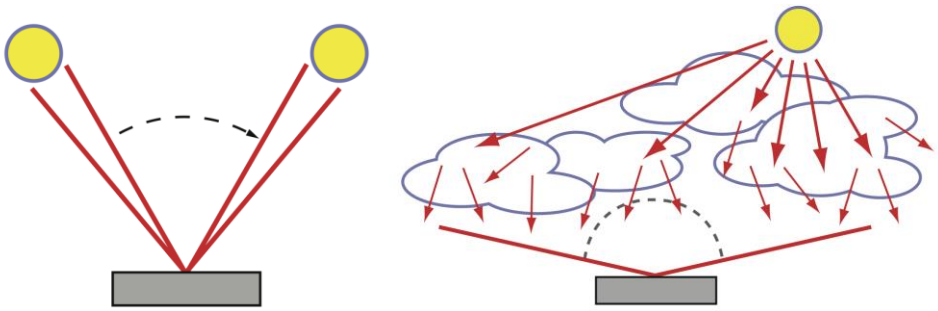

Figure 1.2: Schematics of direct and diffuse angles of incident sunlight striking a solar cell.

1.5 Plasmonics

The unusual optical properties of surface plasmons, the coherent oscillation of electrons on the surface of a metal, have been studied for a number of years. The most famous historical example is the Lycurgus cup from the 4th century AD, which exhibits different colors under reflection and transmission. This unusual optical property was obtained by mixing subwavelength Ag and Au nanoparticles into the glass which scatter green light but transmit red light, resulting in different colors. Quantitative studies of the optical properties of metal nanoparticles began in earnest near the beginning of the 20th century, and were particularly bolstered by Gustav Mie's seminal 1908 paper [6] on the scattering of light by spherical objects, including by Au. In 1957, Ritchie predicted the existence of surface plasmons, and by 1968 Otto, Kretschmann, and Raether had shown that surface plasmons could be excited optically [7, 8, 9]. One of the first major application areas of surface plasmons to emerge was in molecular sensing: rough metallic films were shown to enhance the Raman signal of molecules by several orders of magnitude, and the effect was explained via electromagnetic interactions in references [10, 11]. Discovered in several studies [12, 13, 14, 15, 16, 17, 18] that with advances in nanofabrication, a wide variety of other applications of surface plasmons have emerged in recent years, including optoelectronics components, enhancement of local emitters, materials with negative index of refraction, imaging below the diffraction limit, light emitting diodes, plasmonic lasers, and cancer therapy. While surface plasmons in general exist on any interface of a metal, most research has focused on either localized surface plasmons, such as those on the surface of a nanoparticle, or planar surface plasmons characterized by propagating charge compression waves on the surface. In both cases the wavelengths are small and the electric field intensities high compared to free space.

1.6 Plasmonic Photovoltaics

Inspired by the techniques of optoelectronics, surface plasmons have recently attracted attention for use in solar cells. Indeed, an ultrathin-film solar cell can be considered as an optical integrated circuit, in which light is received, guided, localized, and collected at the nanoscale. The large resonant scattering cross sections of metal nanostructures offer the potential to scatter light strongly, while surface plasmon polaritons can guide and confine light in nanoscale dimensions. The main mechanisms for absorption enhancement in photovoltaics via surface plasmons will be discussed in detail in Chapter 2. The field of plasmonic photovoltaics has emerged in force over the time scale of this thesis, with the number of literature papers and interested commercial manufacturers expanding rapidly, particularly from 2008 onward. The field has benefited greatly from both improved large-area nanofabrication techniques and electromagnetic calculation, which are both discussed throughout this thesis. Studies done in references [19, 20, 22, 23, 24, 25, 26, 27] suggest that to date plasmon-enhanced photocurrent in photovoltaics has been demonstrated in a wide variety of solar cells, including those based on Si, a-Si:H, GaAs, CdSe, InGaN/GaN, InP/InGaAsP, organic semiconductors such as polythiophene and copper pthalocyanine, and hybrid organic-inorganic devices such as dye sensitized solar cells. In parallel, several groups have published theoretical and simulation results on plasmonic solar cell designs.

The design for a PSC varies depending on the method being used to trap and scatter light across the surface and through the material.

I. Nanoparticle cells:

A common design is to deposit metal nanoparticles on the top surface of the thin film SC. When light hits these metal nanoparticles at their surface plasmon resonance, the light is scattered in many different directions. As cited in [28] this allows light to travel along the SC and bounce between the substrate and the nano-particles enabling the SC to absorb more light (fig 1.3(a)). These cells have the advantage that the fabrication process does not have to be substantially modified to incorporate plasmonic scatterers. The disadvantage is that, since the particles are on top, attention must be paid to the density of objects to avoid shadowing. References [29, 30] shows that the presence of particles on top also modifies the use of AR coatings, and so any added benefits from nanoparticles must be weighed against the benefits due to conventional antireflection methods.

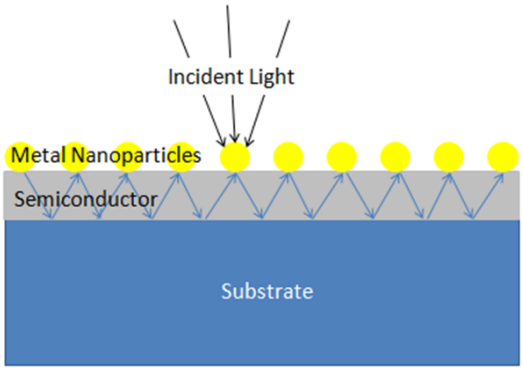

Figure 1.3(a): PSC using metal nanoparticles.

II. Metal film cells:

Other methods utilizing surface plasmons for harvesting solar energy are available. One other type of structure is to have a thin film of silicon and a thin layer of metal deposited on the lower surface. The light will travel through the silicon and generate surface plasmons on the interface of the silicon and metal (fig 1.3(b)). This generates electric fields inside of the silicon since electric fields do not travel very far into metals. If the electric field is strong enough, electrons can be moved and collected to produce a photocurrent. The thin film of metal in this design must have nanometer sized grooves which act as waveguides for the incoming light in order to excite as many photons in the silicon thin film as possible. [31].

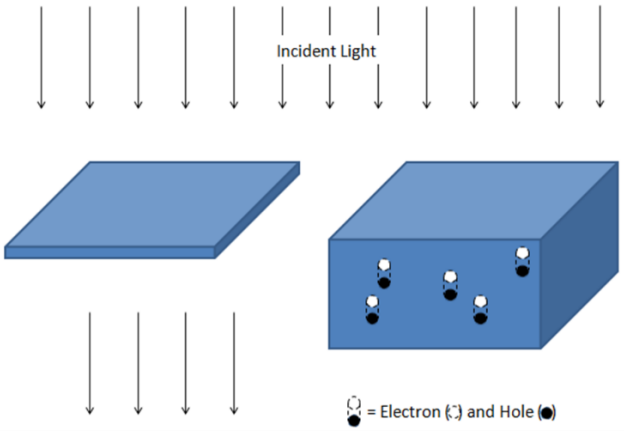

Figure 1.3(b): Thin film SC (left) and Typical SC (right).

1.7 Literature review

In their paper about plasmonic nanoantennas, Vincenzo Giannini, Antonio I. Fernandez, Susannah C. Heck [32] explores rigorously how an incident radiation interacts with metal nanoparticles. When light interacts with a metal nanoparticle its conduction electrons can be driven by the incident electric field in collective oscillations known as localized surface plasmon resonances (LSPRs). These give rise to a drastic alteration of the incident radiation pattern and to striking effects such as the subwavelength localization of electromagnetic (EM) energy, the formation of high intensity hot spots at the NP surface, or the directional scattering of light out of the structure. A. Garcia-Etxarri, R.Gomez-Medina, L.S. Froufe-Perez [33] demonstrates how high-permittivity dielectric particles (e.g. silicon) present strong electric and magnetic dipolar resonances in telecom and near infrared frequencies. Multiple nanoparticles also interacts with each other when placed in close proximity to each other and create enhanced electric field called “Hot Spot”, as explores in the paper published by Katja Erhold, Silke Christiansen and Ulrich Gosle [34]. These nanoparticles and their plasmonic characteristics are good way to create increased absorption in thin-film solar cells. Y. Ekinci, H. H. Solak, and J. F. Löffler [35] shows in their study an engineered enhancement of optical absorption and photocurrent in a semiconductor via the excitation of surface plasmon resonances in spherical Au nanoparticles deposited on the semiconductor surface. N. P. Hylton, X. F. Li, V. Giannini, K. H. Lee, N. J. Ekins-Daukes, J. Loo [36] shows that implementation of metal nanoparticles on GaAs layer can results in increased optical path length and parasitic absorption due to excitation of localized surface plasmon resonances. T. Repan, S. Pikker, L. Dolgov, A. Loot [37] demonstrates in their paper increased efficiency inside the CdTe solar cell absorber caused by plasmonic metal nanoparticles.

Qian Zhou, Debao Jiao, Kailiang Fu, Xiaojie Wu [38] conducted a study on the recently emerging Perovskite solar cells and compares their efficiency with traditional solar cells. Due to their simplicity and low cost, their properties are vigorously studied and researched. Olga Malinkiewicz, Aswani Yella,

Yong Hui Lee, Guillermo Minguez Espallargas, Michael Graetzel [39] shows that methylammonium lead iodide perovskite layers, when sandwiched between two thin organic charge-transporting layers, also lead to solar cells with high power-conversion efficiencies (12%). As researched in the paper published by Wei Zhang, Michael Saliba, Samuel D. Stranks, and Yao Sun, Xian Shi, Ulrich Wiesner, and Henry J. Snaith [40] these perovskite solar also accommodates metal nanoparticles and facilitates field enhancement. Their paper demonstrates photocurrent and efficiency enhancement in mesosuperstructured organometal halide perovskite solar cells incorporating core−shell Au nanoparticles (NPs) delivering a device efficiency of up to 11.4%.

1.8 Overview of Thesis

This thesis describes the design, modeling, and measurement of solar cells incorporating plasmonic nanostructures for enhanced photocurrent. In particular, we focus on plasmonic nanostructures built into the metallic back contact of a thin-film solar cell. In chapter 2 describes rigorously in theoretical details the optical properties of a nanoparticle. Light scattering, localized surface plasmon resonance, surface plasmon polaritons- all these phenomena are discussed and their implementation in solar cell. In chapter 3 electric and magnetic properties of a high-permittivity dielectric particle (Si) are explored. Furthermore in chapter 5 we discussed the arrangement of more than one nanoparticle in close proximity and how they exhibit “Hot Spot”. Chapter 5 and 6 offers insight into the modelling of nanoparticle enhanced solar cell and how field is enhanced in the particle-absorber layer vicinity. Both GaAs and CdTe absorber layer is experimented with many noble metal nanoparticles like Al, Au, Cu, Ag etc. In chapter 7 the recently emerging Perovskite solar cell is explored and how they accommodate metal nanoparticles to enhance their power conversion efficiency.

Chapter 2

Plasmonic Solar Cells

2.1 Introduction

This chapter describes the optical properties of localized and propagating surface plasmons, as applied to photovoltaics. Metals are traditionally seen as recombination centers or sources of optical losses in photovoltaics, and the idea of using metal nanostructures to enhance absorption in solar cells is at first counterintuitive. The unusual properties of plasmonic nanostructures, however, including their scattering cross sections, high local electric fields, and propagating waveguide modes, enable their use in solar cells. This chapter describes the resonant scattering cross-sections of small metal nanoparticles, and considerations when these scatterers are introduced in solar cells. Also the waveguide modes that can be excited in a solar cell, both photonic slab waveguide modes and SPP modes. The challenge for photovoltaic applications is to design scattering objects with high effective cross sections that are both broadband across the solar spectrum and insensitive to angle of incidence.

2.2 Optical properties of metal nanoparticles

Stated in [41, 42] owing to their bright colors, metal nanoparticles (NPs) have been employed for centuries in church windows, mosaics, glass cups, and pottery. This utilization was based on empirical knowledge, without an understanding of the physical origins of the metal NP colors. This however changed, when Gustav Mie published his pioneering work as cited in [43] explaining the optical properties of metal NPs in the beginning of the 20th century. After this theoretical framework had been developed, it took several decades until the advances in the field of nanotechnology led to a widespread use of metal NPs in various research areas. Recently different studies [44-53] discovered and demonstrated potential applications of metal NPs in solar cells, light emitting devices, chemical and biological sensors, surface enhanced Raman spectroscopy, photochemistry, and lasers.

2.3 Localized Surface Plasmon resonances

Studies done in references [54, 55] shows that the unique optical properties of metal NPs arise from the interaction of the NP conduction electrons with the incident light. This interaction can be described by a simplified formalism, the so-called quasistatic approximation, for NPs with a size much smaller than the wavelength (λ) of the incident light. In this size regime, the electric field (E_0) of the light wave is

approximately constant across the entire particle. This spatially constant electric field exerts a force on the conduction electrons of the metal NP, which causes them to collectively move to the NP surface, as shown in Fig. 2.1[56]. At the same time, the Coulomb attraction between these displaced electrons and the ionized metal lattice leads to a restoring force. The combination of these two forces causes a collective oscillation of the electrons with a maximal amplitude at the so-called localized surface plasmon resonance (LSPR) frequency.

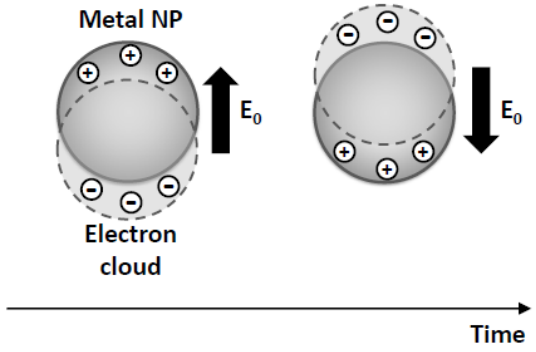

Figure 2.1: Schematic of a dipole LSPR excited in a metal NP with a size much smaller than the wavelength of the incident light with an electric field E_0. This external field exerts a force on the NP conduction electrons, resulting in a collective oscillation. Because of the small NP size, E_0 is approximately spatially constant, resulting in a dipole resonance [56].

In NPs that are small compared to λ , all electrons oscillate in-phase and therefore only dipole LSPRs are excited. As pointed out in references [59-61] these LSPRs should not be confused with surface plasmon polarities (SPPs), which are electromagnetic excitations propagating at the surface of planar metal layers that exhibit evanescent decay in the direction of the surface normal. Unlike SPPs, LSPRs do not propagate (hence the localized in their name) and can be excited by a plane light wave without the need for specific incoupling schemes such as gratings and prisms.

The optical properties of metal NPs are highly dependent on the relative permittivities of the NP material and the embedding medium, ε_{NP} and ε_m, respectively. In general, both of them are complex numbers with $\varepsilon = \varepsilon_1 + i\varepsilon_2$ According to the quasistatic approximation, we only need to know these two material properties as well as the NP radius (R) to calculate the dipole polarizability (α) of a spherical metal NP at a given frequency (ω) of the incident light [56]

$$\alpha(\omega) = 4\pi R^3 \frac{\varepsilon_{np}(\omega) - \varepsilon_m(\omega)}{\varepsilon_{np}(\omega) - 2\varepsilon_m(\omega)} \tag{2.1}$$

The response of the metal NP on the excitation by an external light source can then be described by the induced dipole moment p = $\varepsilon_0 \varepsilon_m \alpha E$, with the vacuum permittivity ε_0. From Eq. (2.1) from [56], it follows that α exhibits resonance behavior whenever

$$| e_{NP} + 2\varepsilon_m | = Minimum \tag{2.2}$$

In a transparent embedding medium, i.e. $\varepsilon_{2,m} = 0$, and for a small $\varepsilon_{2,NP}$ or $\partial\varepsilon_{2,NP} / \partial\omega$, the dipole resonance condition is simplified to [56]

$$\varepsilon_{1,NP} = -2\varepsilon_m \tag{2.3}$$

As shown in references [62, 63], this implies that LSPRs can only be excited if either $\varepsilon_{1,m}$ or $\varepsilon_{1,NP}$ are negative, which necessitates that either the NP or the embedding medium consists of a metal (the latter would correspond to a void in a metal layer, which supports LSPRs as well. The ε_1 of Ag and Au are both negative in the visible spectral range, as shown in Fig.2.2 [56], such that for small spherical NP of these noble metals in vacuum, a dipole LSPR is excited at $\lambda \sim 360$ nm and $\lambda \sim 500$ nm for Ag and Au NPs, respectively.

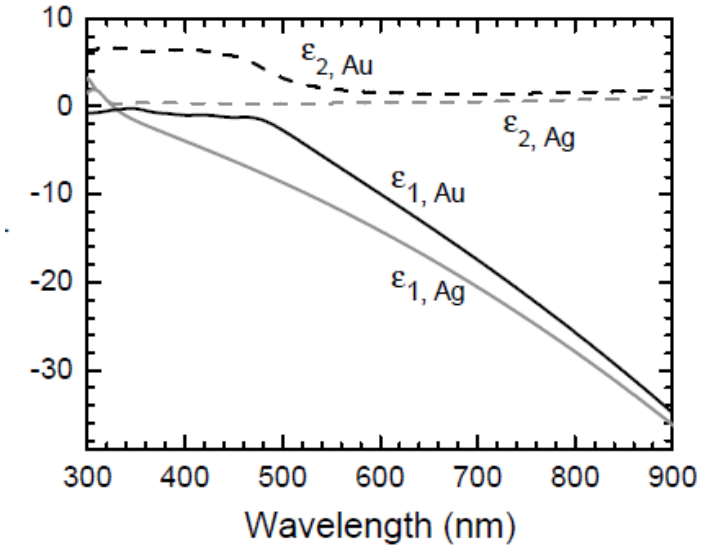

Figure 2.2: Relative permittivities of Ag and Au, as measured by spectroscopic ellipsometry [56].

2.3 Light extinction by metal NPs

Metal NPs exhibit efficient light extinction, which is the sum of light absorption and scattering. These optical properties are a consequence of the LSPRs excited in the metal NPs and have been studied extensively during the last decades. [64-70] have provided evidence that the NP extinction has been found to strongly depend on the NP composition, size, shape, and dielectric environment.

The light extinction, absorption, and scattering of a single metal NP are commonly described by their cross-sections, C_{ext}, C_{abs}, *and* C_{sca}, *respectively*, *with* $C_{ext} = C_{abs} + C_{sca}$. These cross-sections are related to the area within which the metal NP interacts with the incident light. According to the quasistatic approximation, both C_{sca} and C_{abs} of spherical NPs are directly related to α by [56]

$$C_{abs} = k\,\mathrm{Im}(\alpha) \tag{2.4}$$

$$C_{sca} = \frac{k^4}{6\pi}|\alpha|^2 \tag{2.5}$$

where $k = 2\pi\sqrt{\varepsilon_m}/\lambda$ denotes the wavenumber, which is the magnitude of the wave vector (k) of the incident light. It is convenient to normalize these cross-sections by the physical size of the metal NP, such that the normalized cross-sections (Q) for a spherical NP are given by Q = C $/(R^2\pi)$.

The quasistatic approximation is rather accurate for R < 20 nm. Referenced in [71] as proof for NPs with a larger size, the approximation does not hold anymore because phase retardation of the external and internal fields lead to a red-shift of the LSPR and strong light scattering leads to radiation damping . This has also been studied in [72] that in addition, higher-order multipole resonances are excited. All these effects are taken into account in the more rigorous elecrodynamic Mie model cited in [56], where C_{ext} and C_{sca} are given by a multipole expansion of the electromagnetic fields:

$$C_{ext} = \frac{2\pi}{k^2}\sum_{l=1}^{\infty}(2l+1)\,\mathrm{Re}(a_1 + b_1) \tag{2.6}$$

$$C_{sca} = \frac{2\pi}{k^2}\sum_{l=1}^{\infty}(2l+1)(|a_1|^2 + |b_1|^2) \tag{2.7}$$

The so-called Mie coefficients a_1 and b_1, which are given by [56]

$$a_1 = \frac{m\psi_1(mx)\psi'_1(x) - \psi_1(x)\psi'_1(mx)}{m\psi_1(mx)\xi'_1(x) - \xi_1(x)\psi'_1(mx)} \tag{2.8}$$

$$b_1 = \frac{\psi_1(mx)\psi'_1(x) - m\psi_1(x)\psi'_1(mx)}{\psi_1(mx)\xi'_1(x) - m\xi_1(x)\psi'_1(mx)} \tag{2.9}$$

where $x = kR$ and, $m = \sqrt{\varepsilon_{NP} / \varepsilon_m}$ with $\mathrm{Im}(\varepsilon_m) = 0$. ψ_1 and ξ_1 are cylindrical Riccati-Bessel functions, defined by $\psi_1(z) = zj_1(z)$ and $\xi_1(z) = zh_1^{(1)}(z)$, with the spherical Bessel and Hankel functions. The prime indicates differentiation with respect to the argument in parentheses. The order of the multipole is given by l, where the lowest-order mode (l = 1) is a dipole.

Equations (2.5) and (2.6) from [56] allow to extract several general trends for spherical metal NPs. The C_{ext} spectra of a spherical Ag NP with R = 3.5 nm for several ε_m is shown in Fig. 2.3 of [56]. Such small NPs (i.e. $R << \lambda$) exhibit a single extinction band, originating from a dipole LSPR. It red-shifts with increasing ε_m, as expected from the quasistatic dipole resonance condition, Eq. (2.3), and the monotonically decreasing ε_1 of Ag in the visible spectral range (cf. Fig. 2.2, [56]).

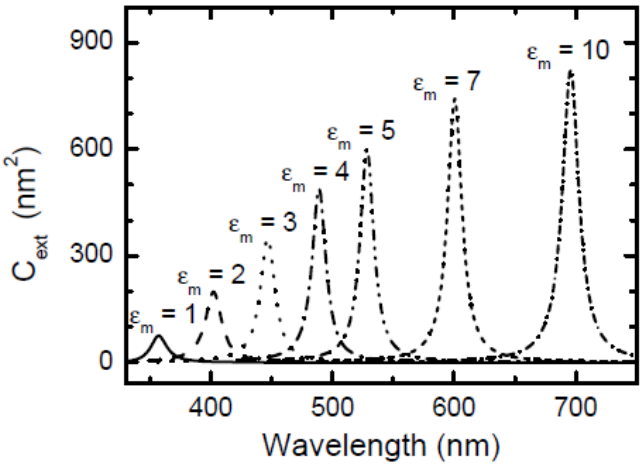

Figure 2.3: Extinction cross-section (C_{ext}) of a Ag NP with R = 3.5 nm for several ε_m, according to Mie theory [56].

The size dependence of extinction, scattering, and absorption of Ag NPs is shown in Fig. 2.4(a)-(c) from [56]. For R = 5 nm, only the dipole LSPR is excited at λ = 360nm [Fig. 2.4(a),]. As the NP size increases, the dipole resonance red-shifts due to phase retardation and becomes broader due to radiative damping [Fig. 2.4(b) and (c)]. For R = 100, for example, the dipole resonance is centered at $\lambda \sim 600$ nm and is highly damped. At the same time, higher-order multipoles are excited at wavelengths smaller than that of the dipole LSPR. The comparison between Q_{scat} and Q_{abs} reveals that for the smallest Ag NPs no significant scattering is observed, whereas it dominates for the larger two NP sizes.

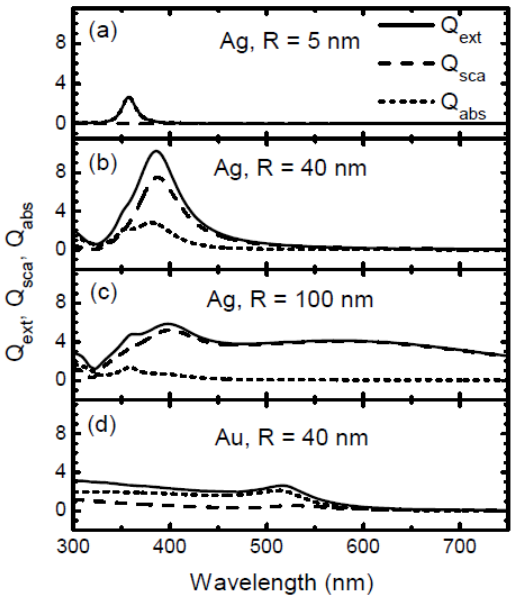

Figure 2.4: Extinction, scattering and absorption efficiencies of spherical (a)-(c) Ag and (d) Au NPs in air for several R, according to Mie theory [56].

Figure 2.5 of [56] shows the dependence of the C_{scat}/C_{ext} ratio on R, according to Mie theory. The growing importance of light scattering with increasing R is also taken into account by the quasistatic approximation, where scattering scales with R^6, whereas absorption only scales with R^3 [Eq. (1.7) and (1.8) from [56]]. The comparison between the C_{scat}/C_{ext} ratio for $\varepsilon_m = 1$ = 1 (solid curve in Fig. 2.5 [56])

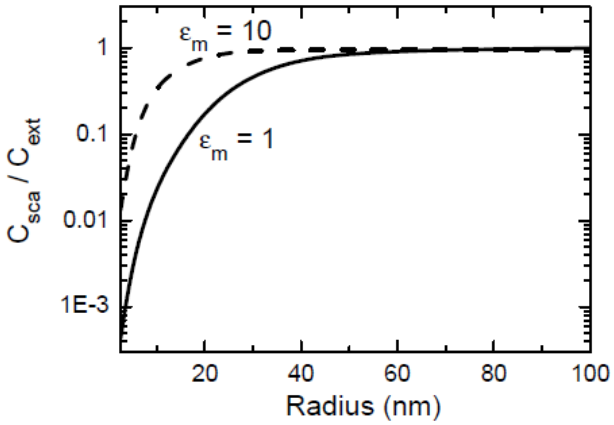

Figure 2.5: The C_{scat} / C_{ext} ratios for a Ag NP with a radius R in an embedding medium with ε_m = 1 (solid curve) and ε_m = 10 (dashed curve), according to Mie theory [56].

and ε_m = 10 (dashed curve) shows that the importance of light scattering for a given R strongly increases with increasing ε_m.

Finally, we can consider the role of the NP material composition itself. In the visible spectrum, Ag absorbs only very little light, resulting in a small ε_2 (cf. Fig. 2.2 [56]). Gold, on the other hand, absorbs more strongly due to interband transitions that extend into the visible spectral range. This is evidenced by the much weaker resonance and less effective light scattering of Au NPs compared to Ag NPs of the same size, as shown in Fig. 2.4(d) of [56].

So far, we have only discussed the optical properties of spherical metal NPs. Studies for non-spherical metal NPs [73-76] suggest they also have optical properties that strongly depend on their shape. Rod-shaped particles, for example, exhibit one dipole LSPR per non-degenerated axis as found in reference [77], as shown by the experimentally measured spectra of Au NPs in Fig. 2.6 [56]. The optical properties of such rather simple non-spherical geometries can still be calculated analytically. For more complicated geometries, however, numerical simulations have to be employed. The quasistatic and Mie models described above both rely on ε as their only material-related parameter. Therefore, the results obtained from these models can only be as accurate as the ε values that are utilized for the calculations. Because ε is a macroscopic material property, the models neither take into account the damping of the electron oscillation when the NP size is smaller than the mean free path length of the electrons nor nonlocal effects at the metal-dielectric interface, that both become increasingly important with decreasing NP size. Although models exist that take these effects into account [78], they require the detailed knowledge about microscopical parameters such as the exact morphology of the metal NP/embedding medium interface and the shape and size distribution of the NPs. As in real-life experiments, these parameters are mostly unknown or could only be roughly estimated, the benefit of utilizing models that correct for surface scattering and nonlocal effects is not obvious.

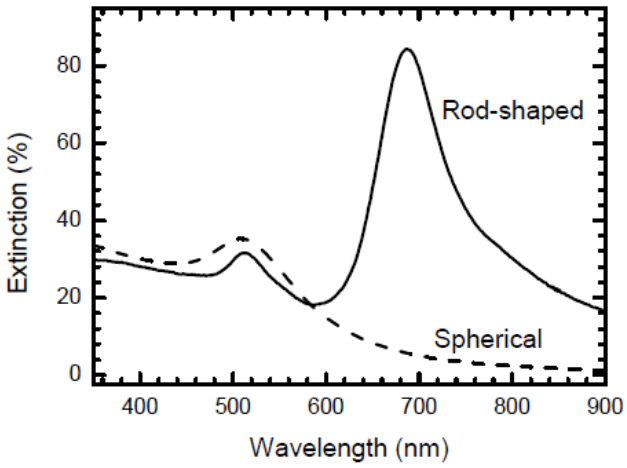

Figure 2.6: Experimentally measured extinction spectra of colloidal dispersions of spherical Au NPs with R□ 5 nm (dashed curve) and rod-shaped Au NPs with a minor axis diameter of 10 nm and a 3:1 aspect ratio (solid curve) [56].

2.4 Metal NP-embedding medium Interactions

The excitation of LSPRs in a metal NP leads to a strong enhancement of the electric field intensity ($|E|^2$) near its surface. This enhancement depends on the metal NP shape and the position relative to the E_0 vector of the incident light wave, as shown by Fig.2.7 showed in [56]. In the quasistatic approximation, the near-field intensity enhancement ($|E_{NP}|^2 / |E_0|^2$) at the distance d to the surface of a metal

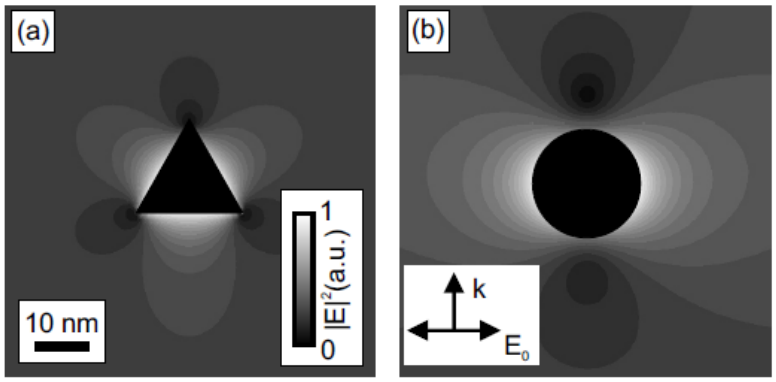

Figure 2.7: Normalized electric field intensity ($|E|^2$) near Ag NPs with a (a) triangular and (b) circular cross-section, as obtained by 2D numerical simulations. The plane light wave is incident from the bottom, with its E_0 and k vectors as indicated by arrows [56].

NP with radius R is given by [79]

$$\frac{|E_{NP}|^2}{|E_0|^2} = |1+\frac{\alpha}{2\pi(R+d)^3}|^2 \cos^2\theta + |-1+\frac{\alpha}{2\pi(R+d)^3}|^2 \sin^2\theta \quad (2.10)$$

where $|E_{NP}|$ denotes the electric field intensity outside of the metal NP and θ the angle between the E_0 vector of the incident light and the vector pointing from the NP center to the point of interest. The maximal field enhancement is obtained for θ = 0, π. At these angles, Eq. (2.9) from [56] can be simplified to [56]

$$(\frac{|E_{NP}|^2}{|E_0|^2})_{\max} = |1+\frac{\alpha}{2\pi(R+d)^3}|^2 \quad (2.11)$$

Shown in references [80-83] that as a result of this near-field enhancement, the absorption in the embedding medium can be strongly increased due to the presence of metal NPs. Below saturation, this absorption enhancement equals $\frac{|E_{NP}|^2}{|E_0|^2}$.

In addition to near-field enhancement, light scattering by metal NPs can also lead to absorption enhancement in thin-films due to light trapping. Light scattering by metal NPs only becomes efficient for NPs with a size above $\sim$30-50 nm, whereas the near-field enhancement can already be very strong even for NPs with a size of only a few nm.

The presence of metal NPs does not only affect light absorption in the embedding medium but also the PL of nearby emitters such as organic molecules and semiconductor nanocrystals. Several studies cited in [84-98] demonstrate that Metal NPs have been found to either strongly quench or enhance the PL of nearby emitters, depending on the size, shape, composition, and dielectric environment of the metal NPs, the natural quantum yield of the emitter, the distance between the NPs and the emitter, and the spectral overlap of the LSPR and the emission. Also as discovered in different studies cited in [99, 100, 101–103], the effect of the presence of metal NPs on the PL of nearby emitters originates from both the absorption enhancement that corresponds to an excitation enhancement in the context of PL measurements, as well as a modulation of the emission quantum yield and a reduction of the excitation lifetime.

2.5 Overview of Mechanisms for Plasmonic Absorption Enhancement

There are a few distinct plasmonic mechanisms for enhancing absorption in solar cells, which together encompass most of the explored devices to date. First, subwavelength metal nanostructures (on either the front or back of an absorbing layer) can be used to scatter incident light into a distribution of angles, increasing the path length of the light within the absorbing layer (Fig. 2.8(a)) from [56]. Evidence in [104,

105] points out that this can lead to higher short circuit current densities, in both relatively thick cells and thin cells on index-matched substrates.

A second plasmonic mechanism for enhanced absorption results from high near-field intensities associated with the localized surface plasmonic resonance of the particle (Fig. 2.8(b)). Depending on the shape and size of a metallic particle, particular frequencies of optical excitation will result in strongly enhanced fields near the particle.

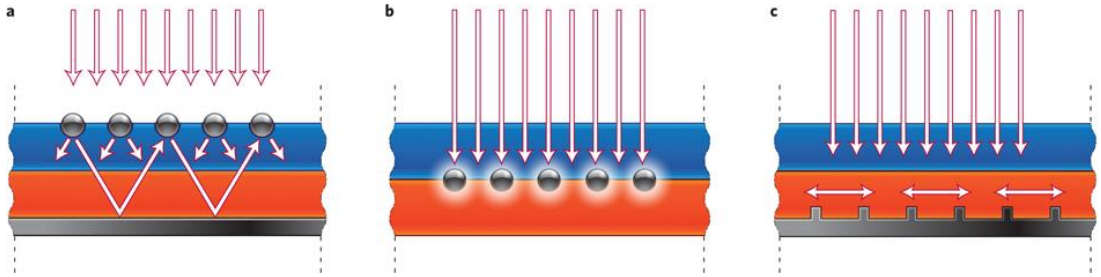

Figure 2.8: (a) Light trapping by nanoparticles from metal nanoparticles on the top surface of the solar cell. Light is scattered and trapped into the substrate at a higher angle, increasing the path length. (b) Light absorption enhancement in the semiconductor by embedded nanoparticles due to the enhanced near field of the nanoparticles. (c) Light trapping by coupling to guided modes of the solar cell from nanopatterned metallic back contacts

Since the optical absorption is proportional to the field intensities, high local fields lead to increased absorption. This can be a challenging geometry, however, as the embedded metal particles can lead to semiconductor defects or act as recombination centers, in addition to the fabrication challenges. A study cited in [106] demonstrates that most of the successful solar cells of this geometry are polymer devices, where metal particles can be incorporated through spin-casting.

The third mechanism uses the scattering center as a means to excite propagating waveguide modes within the thin absorbing layer (Fig. 2.8(c)). [107-110] have mentioned that the propagating waveguide modes may be either photonic waveguide modes or surface plasmon polariton (SPP) modes, and the scattering center is used to overcome the momentum mismatch between the incident wavevector and that of the waveguide mode. As the mode propagates, the power in the waveguide mode will be absorbed partially in the semiconductor layer, thereby exciting electron-hole pairs and enhancing absorption by redirecting the light horizontally. Carrier collection usually occurs in the vertical direction, orthogonal to the absorption path. This third design is the focus of most of this thesis. Figure 2.9 from ref. [56] illustrates several possible architectures for integrating scattering objects into photovoltaic devices.

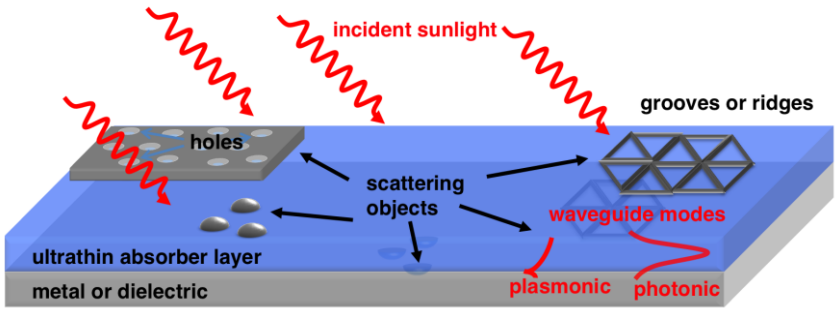

Figure 2.9: Generalized scatterers for coupling into waveguide modes in a solar cell, showing some of the potential variables for designing plasmonic nanostructures. Scatterers can consist of particles on top, middle, or back of the solar cell and could contain layers of metal, dielectrics, transparent conducting oxides, or air. Incident sunlight is scattered into photonic or SPP modes depending on the scattering object and incident wavelength of light.

Variables include the shape of the scattering center, its relative height in the waveguide, arrangement with respect to other scattering objects, and the use of either dielectric or metallic surrounding layers. For example, the scattering objects may be nanoparticles, gratings, or holes in an otherwise continuous metal film. The shape of the nanostructure is another variable: hemispheres, cylinders, cones, or anisotropic shapes are all possibilities, each with their own scattering cross section and angular scattering distribution.

Chapter 3

Scattering Properties of a single silicon nanoparticle in air

3.1 Introduction

Here we analyze the dipolar electric and magnetic response of lossless dielectric spheres made of moderate permittivity materials. For low material refractive index ($\leq$3) there are no sharp resonances due to strong overlapping between different multipole contributions. However, we find that Silicon particles with index of refraction $\sim$ 3.5 and radius $\sim$200nm present strong electric and magnetic dipolar resonances in telecom and near-infrared frequencies, (i.e. at wavelengths ≈ 1.2−2mm) without spectral overlap with quadrupolar and higher order resonances. The light scattered by these Si particles can then be perfectly described by dipolar electric and magnetic fields.

3.2. Extinction resonances of a dielectric sphere. The Mie theory revisited

Consider a non-absorbing dielectric sphere of radius a, index of refraction m_p and dielectric permittivity $\varepsilon_p = m_p^2$ in an otherwise uniform medium with real relative permittivity ε_h , permeability $\mu_h = 1$, and refractive index $m_h = \sqrt{\varepsilon_h}$. The magnetic permittivity of the sphere and the surrounding medium is assumed to be 1. Under plane wave illumination, and assuming linearly polarized light, the incident wave is described by

$$E = E_0 u_z e^{ikX} e^{-i\omega t} \tag{3.1}$$

$$B = B_0 u_y e^{ikX} e^{-i\omega t} \tag{3.2}$$

where $k = m_h \omega / c = m_h 2\pi / \lambda, \lambda$ being the wavelength in vacuum and $B_0 = \mu_0 H_0 = -(m_h / c) E_0$ (see Fig. 3.1). The field scattered by the sphere can be decomposed into a multipole series, (the so-called Mie's expansion), characterized by the electric and magnetic Mie coefficients $\{a_n\}$ and $\{b_n\}$, respectively; (a_1 and b_1 being proportional to the electric and magnetic dipoles, a_2 and b_2 to the quadrupoles, and so on).

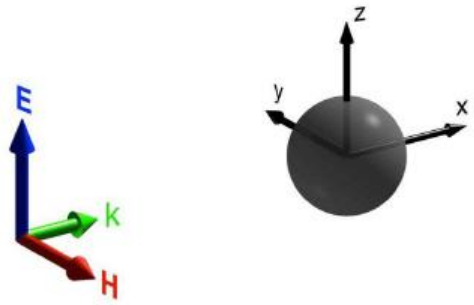

Figure 3.1: Incident field vector [36].

We shall find useful to write the Mie coefficients in terms of the scattering phase-shifts α_n and β_n [112]

$$a_n = \frac{1}{2}(1 - e^{-2i\alpha_n}) = i \sin \alpha_n e^{-i\alpha_n} \tag{3.3}$$

$$b_n = \frac{1}{2}(1 - e^{-2i\beta_n}) = i \sin \beta_n e^{-i\beta_n} \tag{3.4}$$

Where

$$\tan \alpha_n = \frac{m^2 j_n(y)[x j_n(x)]' - j_n(x)[y j_n(y)]'}{m^2 j_n(y)[x y_n(x)]' - y_n(x)[y j_n(y)]'} \tag{3.5}$$

$$\tan \beta_n = \frac{j_n(y)[x j_n(x)]' - j_n(x)[y j_n(y)]'}{j_n(y)[x y_n(x)]' - y_n(x)[y j_n(y)]'} \tag{3.6}$$

$m = m_p / m_h$ being the relative refractive index, $x = ka$ the size parameter and $y = mx$. $j_n(x)$ and $y_n(x)$ stands for the spherical Bessel and Neumann functions, respectively, and the primes indicate differentiation with respect to the argument. Discussed in [112], in absence of absorption, i.e. for real m, the phase angles α_n and β_n are real, then the extinction and scattering cross sections, σ_{ext} and σ_s, respectively, have the common value

$$\sigma_s = \sigma_{ext} = \frac{2\pi}{k^2} \sum_{n=1}^{\infty} (2n+1)\{\sin^2 \alpha_n + \sin^2 \beta_n\} = \sum_{n=1}^{\infty} \{\sigma_{E,n} + \sigma_{M,n}\} \tag{3.7}$$

In the small particle limit (x ≪ 1) and large particle permittivities (m ≫ 1) the extinction cross section presents characteristic sharp resonance peaks. The values of y = mx at which the angles α_n or β_n are

π /2, $3\pi/2$, . . ., etc., define the resonance points. At each resonance, the extinction cross section is of the order of λ^2 and it is independent of either the particle size or the refractive index [112]

$$\sigma_S^{res} = \sigma_S^{ext}\{x << 1; m >> 1\} \approx \frac{2\pi}{k^2}(2n+1) \tag{3.8}$$

Asymptotically, the first resonance peak occurs at y = π (i.e. λ = m2a) corresponding to the magnetic dipole term of coefficient b_1 .

3.2 Magnetic and electric resonances of dipolar particles

Let us consider further in some detail the scattering properties of small dielectric particles (x ≪ 1). In the x ≪ 1 limit, the sphere is sufficiently small so that only the dipole scattered fields are excited. The induced dipole moments, proportional to the external (polarizing) fields, **E** and **B**, are usually written in terms of the particle electric and magnetic polarizabilities α_E and α_M , respectively [112]

$$p = \varepsilon_0 \varepsilon_h \alpha_E E, \; m = \frac{1}{\mu_0 \mu_h}\alpha_M B \tag{3.9}$$

Where

$$\alpha_E = i(\frac{k^3}{6\pi})^{-1} a_1, \; \alpha_m = i\left(\frac{k^3}{6\pi}\right)^{-1} b_1 \tag{3.10}$$

By using the definition of the phase angles α_1 and β_1 , [cf. Eqs. 3.3-3.6], we can rewrite the polarizabilities as [112]

$$\alpha_E = \frac{\alpha_E^{(0)}}{1 - i\frac{k^3}{6\pi}\alpha_E^{(0)}} \;, \; \alpha_M = \frac{\alpha_M^{(0)}}{1 - i\frac{k^3}{6\pi}\alpha_M^{(0)}} \tag{3.11}$$

Where

$$\alpha_E^{(0)} = -\frac{6\pi}{k^3}\tan\alpha_1 \;, \; \alpha_M^{(0)} = -\frac{6\pi}{k^3}\tan\beta_1 \tag{3.12}$$

In terms of these magnitudes, the extinction and scattering cross sections then read

$$\sigma_{ext} = k\,\mathrm{Im}\{\alpha_E + \alpha_M\} \tag{3.13}$$

$$\sigma_S = \frac{k^4}{6\pi}\{|\alpha_E|^2 + |\alpha_M|^2\} \tag{3.14}$$

Of course, in absence of absorption, $\alpha_E^{(0)}$ and $\alpha_M^{(0)}$ are real quantities and we recover the well-known optical theorem result $\sigma_{ext} = \sigma_s$ In particular, in the Rayleigh limit, when $y = 2\pi ma / \lambda << 1, \alpha_E^{(0)}$ and $\alpha_M^{(0)}$ approach the quasi-static form [112]

$$\alpha_E^{(0)}|_{y<<1} \approx 4\pi a^3 \frac{m^2-1}{m^2+1}, \quad \alpha_M^{(0)}|_{y<<1} \approx 4\pi a^3 (m^2-1)\frac{k^2 a^2}{30} \qquad (3.15)$$

From studies cited in [113-115], we recover the well-known expression for the polarizability of a Rayleigh particle including radiative corrections. Notice that in this limit the magnetic polarizability is negligible. Very small particles always behave as point electric dipoles.

However, for particle sizes that are not extremely subwavelength, the quasi-static approach fails to describe the resonant behavior. As y increases, (i.e. as l decreases), there is a crossover from electric to magnetic behavior as shown by Fig. 3.4 for a Si particle. The y values at which the quasi-static polarizability $\alpha_E^{(0)}$ ($\alpha_M^{(0)}$) diverges define the electric (magnetic) dipolar resonances.

Near the first b_1-resonance, the particle essentially behaves like a magnetic dipole. If λ decreases further, a_1 peak dominates and the sphere becomes again an electric dipole. Notice however that, due to the overlap between the electric and magnetic responses, the radiation field near the resonances does not correspond to a fully pure electric or a fully pure magnetic dipolar excitation. Yet, for the aforementioned Si sphere, the magnetic dipole contribution is, at its peak, about five times larger than the electric dipole one.

3.3 COMSOL Simulation Settings

Fig 3.2 shows our COMSOL simulation structure with a cross-section of the 3-D model a single Silicon nanoparticle in air. The radius of the nanoparticle is taken 230nm. The region outside of the nanoparticle is air. A perfectly matched layer (PML) is taken outside of the region of interest which is at least 3 times the radius of the nanoparticle. The incident field decays completely inside the PML layer.

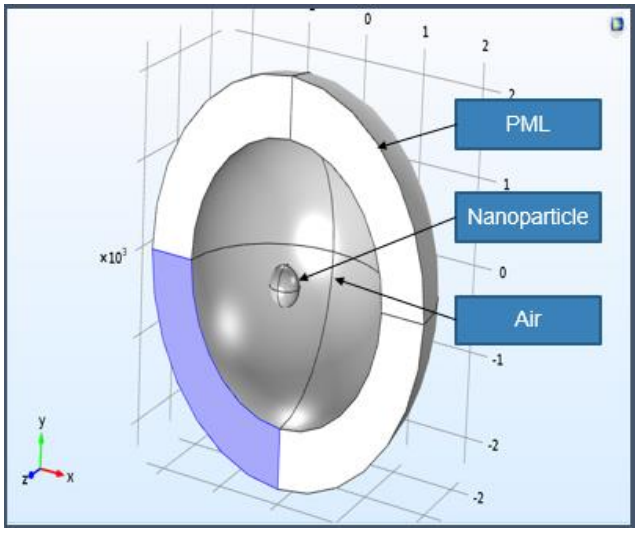

Figure 3.2: Cross-section of the 3-D COMSOL simulation

3.4 Maps for the modulus of the total electric vectors normalized to the incoming Electric field (E_{tot} / E_{inc})

Fig 3.3 shows the total electric field vectors normalized to the incoming electric field (E_{tot} / E_{inc}). XZ planes crossing y=0 are displayed. Field vectors are shown at $\lambda = 1250nm$ where the electric resonance peak occurs (fig 3.3(a)), $\lambda = 1680nm$, where magnetic resonance peak occurs(fig 3.3(b)) and at $\lambda = 1525nm$, where electric and magnetic field contribute equally in the scattering cross-section(fig 3.3(c)).

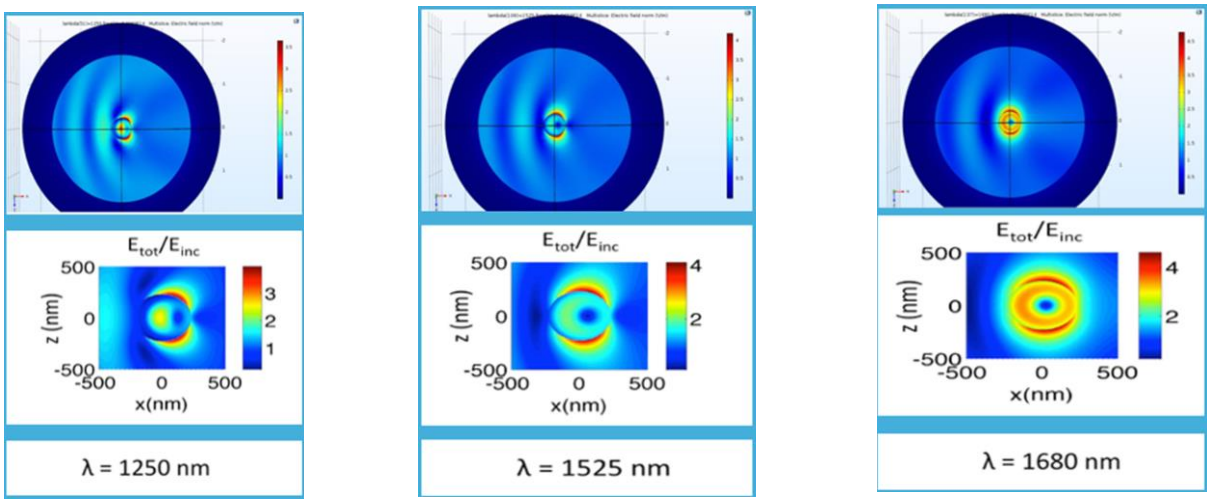

(a) (b) (c)

Figure 3.3: Normalized electric field (E_{tot} / E_{inc}) during (a) electric resonant peak ($\lambda = 1250$nm), (b) magnetic resonant peak ($\lambda = 1525$nm), (c) electric and magnetic field at equal magnitude ($\lambda = 1680$nm)

3.5 Maps for the modulus of the total electric vectors normalized to the incoming Magnetic field (H_{tot} / H_{inc})

Fig 3.4 shows the total magnetic field vectors normalized to the incoming electric field (H_{tot} / H_{inc}). XZ planes crossing y=0 are displayed. Field vectors are shown at $\lambda = 1250nm$ where the electric resonance peak occurs (fig 3.4(a)), $\lambda = 1680nm$, where magnetic resonance peak occurs (fig 3.4(b))and at $\lambda = 1525nm$, where electric and magnetic field contribute equally in the scattering cross-section (fig 3.4(c)).

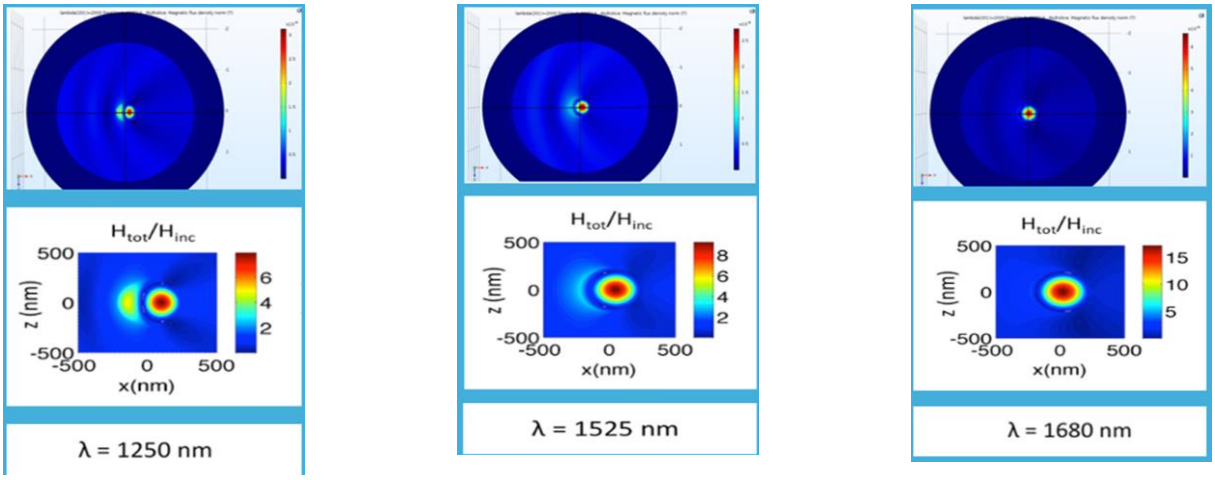

(a) (c) (b)

Figure 3.4: Normalized magnetic field (H_{tot} / H_{inc}) during (a) electric resonant peak ($\lambda = 1250$nm), (b) magnetic resonant peak ($\lambda = 1525$nm), (c) electric and magnetic field at equal magnitude ($\lambda = 1680$nm)

3.6 Far-field radiation pattern and scattering radiation cross-sections vs. wavelength characteristics

Fig 3.5 shows the corresponding far-field scattering radiation patterns for the three wavelengths. Also the scattering cross section σ_s versus the wavelength λ for a 230nm Si sphere is show in following figure (fig (3.6)).

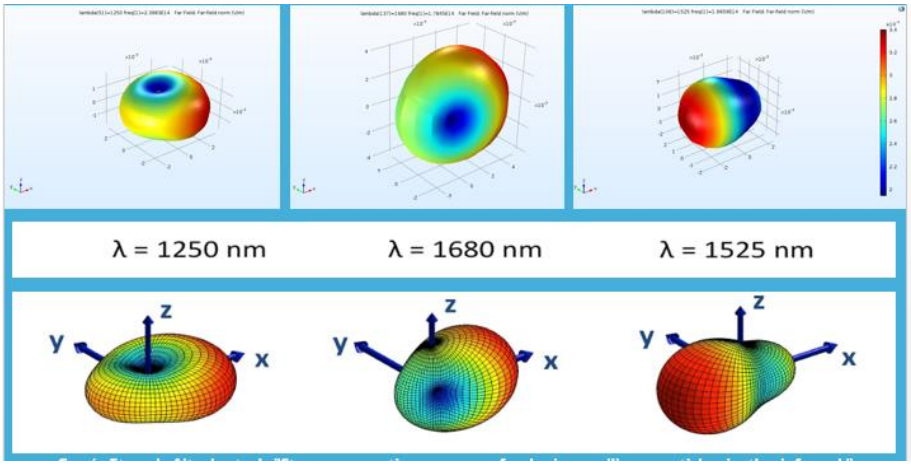

Figure 3.5: The corresponding far field scattering radiation patterns for the three wavelengths

The contribution of each term in the Mie expression is also shown. From the graph we notice that as we increase the wavelength along right x-axis, electric and magnetic dipoles and multipoles occur alternately. Our simulation result accurately matches with the journal paper.

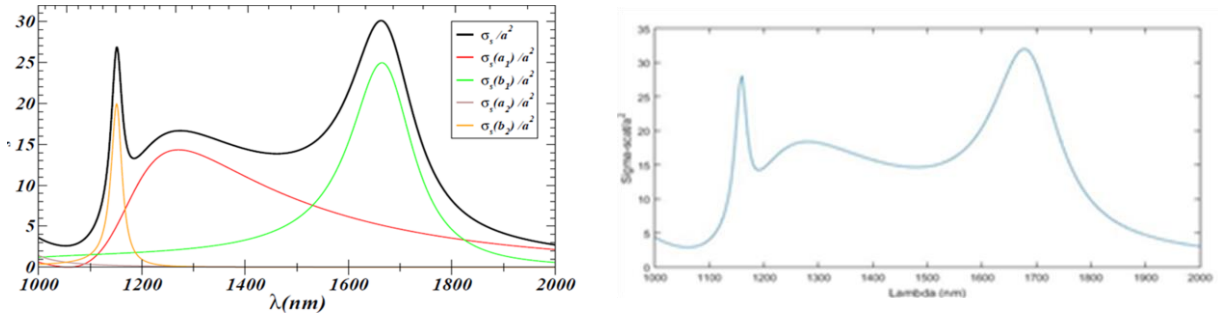

(a) (b)

Figure 3.6: Graph of scattering cross-section versus wavelength (λ) showing (a) alternating magnetic and electric field peak values at 1180 nm , 1250nm ,1680 nm (b) our simulation result

Chapter 4

Plasmonic Properties of Bimetal Nanoshell Spheres

4.1 Introduction

The dimer structures ensure the existence of a so-called hot spot, where the local electric field enhancement reaches its maximum. The hot spot is located in-between the dimer junction and is caused by the coupling of the two particle's plasmon modes. The nanoantenna geometry under analysis is depicted in Fig. 4.1, and it consists of a plasmonic dimer of total length L composed of two spherical nanoparticles separated by a gap of length $g \ll L$. Even if the total size of the nanoantenna is supposed to be of a few tens of nanometers, its size remains comparable with the optical wavelength of operation. One should also keep in mind that this point dipole approximation underestimates particle interactions at close separations. However, the picture is still useful in providing some insight into the interaction phenomenon. Although particle dimmers create hot spots, the electric field intensity enhancement is generally quite low.

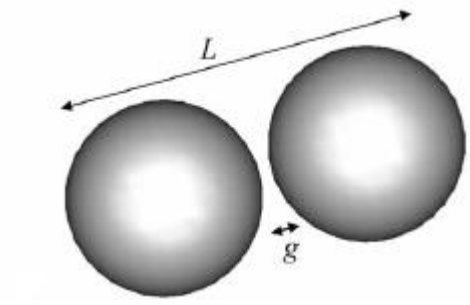

Figure 4.1: The nanoantenna geometry under analysis here

In our COMSOL simulation, we have used two dimetal dishell (fig 4.2) nanoparticles, where the inner core is made of Au and outer shell Ag. We have taken the radius of the core (Au) 40nm and the width of the outer shell (Ag) is 10nm. The outer region of integration includes air (dielectric). A Perfectly Matched Layer (PML) of thickness 150 nm and radius 500nm is also taken.

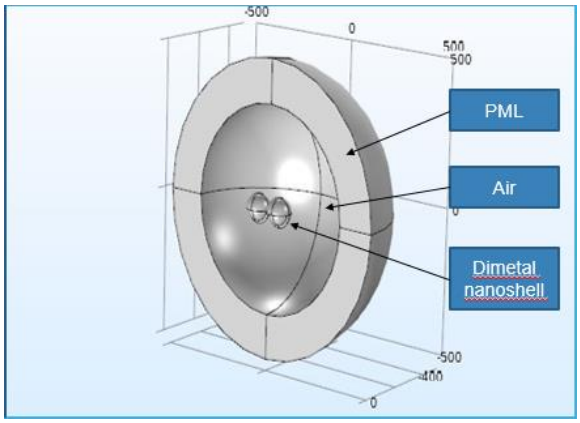

Figure 4.2: Cross-section of the 3D COMSOL simulation

4.2 Electric field distribution and Scattering cross-section

As evidenced by Fig 4.3, due resonant plasmonic interaction between the two dimetal dishells, the electric field in the vicinity between the shells is profoundly increased. This is called a “HOT SPOT”.

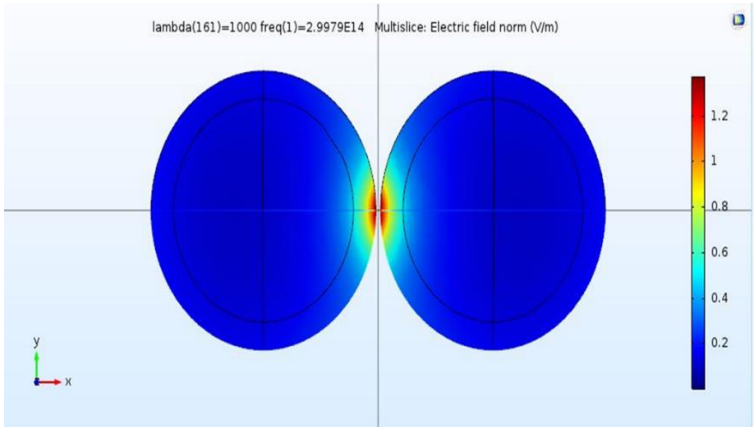

Figure 4.3: Enhanced electric field in between the dimer structure called “Hot Spot”

This hot spot shows a maximum peak at a wavelength, $\lambda = 645$nm as seen in the scattering cross-section vs. wavelength characteristics of the dimetal dishell nanoparticle in fig 4.4

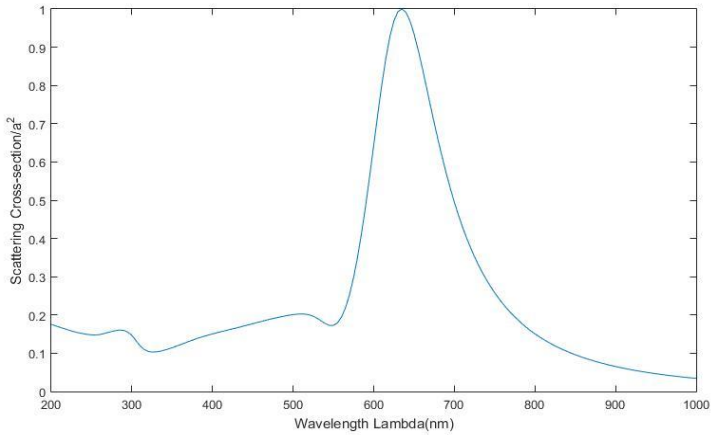

Figure 4.4: Graph of scattering cross-section (σ_{scat} / a^2) vs. wavelength (λ) showing peak electric field at λ =645nm.

Chapter 5

Metal Nanoparticle Enhanced Light Absorption in GaAs Thin-Film Solar Cell

5.1 Introduction

Thin-film solar cells is an emerging technology and has the potential to reduce the cost of current photovoltaic cells. For increasing the light absorption and therefore cell efficiency, light trapping plays a particularly critical role in thin-film solar cells. Light trapping is performed in conventional Si solar cells by utilizing a pyramidal surface structure that scatters the light into the cell and thus increases the effective path length [116-118]. Optically thick photovoltaic (PV) layers are required to design considerably high efficiency PV cells, while the minority carrier diffusion lengths should be kept several times the material thickness to permit effective carrier collection [119]. Therefore, reducing the material usage while increasing the cell efficiency can be achieved by decreasing the PV active region thickness while maintaining the optical thickness. One way of achieving this is by incorporating metallic nanoparticles in the absorber layer of the PV cell. In recent years, plasmonic nanoparticles coupled to semiconductors have been exploited to improve the light absorption in thin-film solar cells [120-124]. Increase in absorption with the help of metal nanoparticles can be achieved in two ways. Firstly, by scattering the incoming light, optical path length can be increased and light trapping can be achieved. Secondly, by enhancement of absorption caused by strong local fields due to the plasmon resonance of the particle [122, 125]. The optical path enhances when the light beam inside the film goes through total internal reflections at the layer's interface. This is only possible for light propagating inside the film at angles more than the critical angle. The antenna-like response of the nanoparticle also plays a significant role for increasing the material extinction of the incident light (caused by the locally enhanced electromagnetic field at the surface plasmon resonance in the vicinity of the nanoparticles) as well as enhanced scattering cross section for off resonant light.

Due to the collective oscillation of the metal's conduction electrons, metal nanoparticles behave as powerful scatterers of light in wavelengths close to the surface plasmon resonance. For effectively point particles, or particles with diameters considerably below the wavelength of the light, the absorption and scattering of light is described by a point dipole model. The model describes the scattering and absorption cross-section as [126]:

$$C_{scat} = \frac{1}{6\pi}\left(\frac{2\pi}{\lambda}\right)|\alpha|^2, C_{abs} = \frac{2\pi}{\lambda}\mathrm{Im}[\alpha] \tag{5.1}$$

Where

$$\alpha = 3V\left[\frac{\varepsilon_p / \varepsilon_m - 1}{\varepsilon_p / \varepsilon_m - 1}\right] \tag{5.2}$$

is the particle's polarizability. Here V denotes the volume of the particle, ε_p the particle's dielectric function and ε_m expresses the dielectric function of the medium the particle is inside. It is evident that when $\varepsilon_p = -2\varepsilon_m$ the nanoparticle's polarizability will become considerably large. This particular scenario is known as the surface plasmon resonance. The scattering cross-section can well surpass the geometric cross-section of the particle at the surface plasmon resonance.

This study concentrates on the effects of the near-field enhancements of the metal nanoparticles (NP) on the GaAs absorber layer due to surface plasmon resonance. A large portion of the solar spectrum is absorbed poorly by thin film solar cells, especially in the intense 600-1100 nm region [125]. Thus, the impact of metal nanoparticles of Gold (Au), Silver (Ag), Copper (Cu) and Aluminum (Al) were studied using the finite element computer simulation software COMSOL Multiphysics and the absorption of GaAs in each case was compared, in the 500-800 nm spectral range. The light absorption and its enhancement is also dependent on the size of the nanoparticles inside the absorber layer. Varying the diameter of the embedded nanoparticles, their effects on light absorption on the GaAs absorber layer was also studied for application in thin-film solar cell technology.

5.2 Simulation Settings

The Scattered field formulation for the nanoparticles are solved by the finite element method simulation software COMSOL Multiphysics 5.2. As the scope of this work was mainly focused on the near field effects of plasmonic nanoparticles, simulations were performed to calculate the absorption in GaAs in the vicinity of the nanoparticle surface. Unwanted additional effects, e.g. interference may affect the simulation while simulating the whole solar cell structure. To simplify and calculate the plasmonic interaction of the near field and differentiate it from other effects superfluous to our study, we used the 3D simulation geometry as depicted in Fig. 5.1. The energy absorbed by the GaAs absorber was calculated by integrating the absorption in a 20nm GaAs layer immediate to the metallic nanoparticle. A maximum mesh size of 30 nm was used.

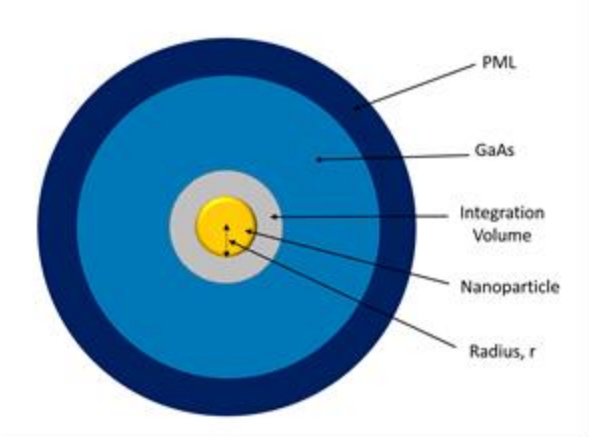

Figure 5.1: Simulation Structure with metallic NP at center surrounded by a 20nm GaAs Volume of Integration (absorption calculation made here), followed by a buffer region of GaAs of 80nm. At the boundary a 30nm PML region is present.

Perfectly matched layers (PML) of 30nm was set up along the boundary of the simulation space. The main purpose of the PML is to strongly absorb the outwardly propagating electromagnetic waves from the interior of a computational region without reflecting them back. A space of about 80nm of GaAs was kept between the PML and the Absorbing region of interest so that the strong near fields may fully diminish before interacting with the PML which might cause severe distortions [127].

For obtaining the absorption enhancement, the absorption in the integrating volume of GaAs surrounding the nanoparticle was divided by the reference absorption of the GaAs without the presence of the nanoparticle. The reference absorption is calculated by integrating the total absorption in the integrating volume of interest and the nanoparticle volume without the presence of any foreign metallic nanoparticle. The wavelength range of 400 nm to 800 nm was included in the work because the GaAs has a bandgap of 1.43 eV (which corresponds to 867nm) and the absorptance (k) of GaAs is negligible above a wavelength of about 830 nm. The optical constants of gold, silver and copper was taken from [128], aluminum from [129] and optical constants of GaAs layer from [130].

5.3 Comparison of Metal Nanoparticles

A reference absorption lower than the absorption in the presence of a metallic nanoparticle within the GaAs volume of interest suggests an enhancement of absorption with the aid of that nanoparticle. For an Au nanoparticle of radius 25 nm, the absorption in the GaAs absorber layer with and without the presence of the nanoparticle is illustrated in the

Fig. 5.2. The absorption in the nanoparticle and the absorption in the GaAs layer adjacent to the nanoparticle were determined independently and correspond to the yellow and blue colored area respectively. The reference absorption is also indicated in dotted lines for comparison. For wavelength greater than 710nm, the Au nanoparticle is effective in the GaAs media as the reference absorption of

GaAs is lower than that with the presence of Au nanoparticles in this spectral range. This can more easily be seen from the absorption enhancement in Fig. 5.6, where the absorption enhancement of more than 1 is evident above 710nm.

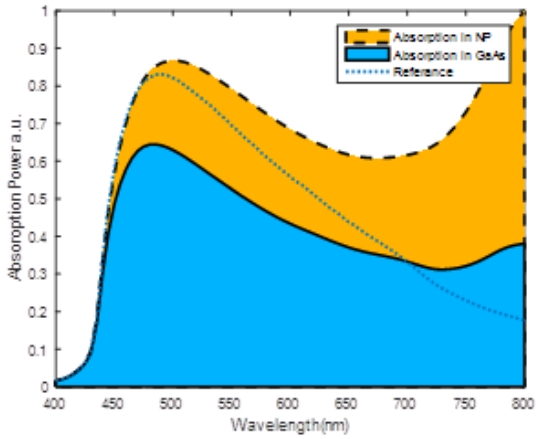

Figure 5.2: The influence of a 25nm radius Au NP on the light absorption with in the GaAs absorber layer. The dotted line is the reference absorption without the NP in the same volume of absorption

With Ag nanoparticles, the absorption in the GaAs layer is more than the reference absorption above 675 nm wavelength as depicted in Fig. 5.3. It is apparent from Fig. 5.6 that the absorption enhancement lies above 1 when the wavelength is above 675 nm

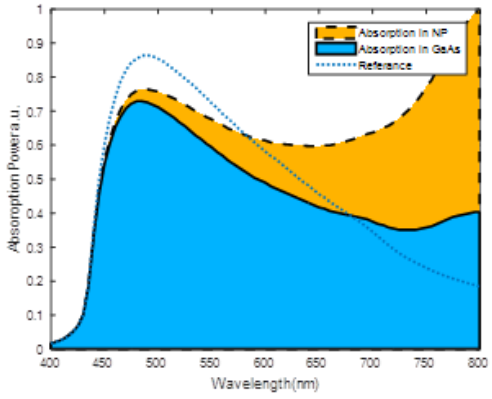

Figure 5.3: The influence on the light absorption of a 25nm radius Ag NP in the GaAs absorber layer. The dotted line is the reference absorption without the NP in the same volume of absorption

Likewise, Cu nanoparticles also shows a similar type of result. The absorption in the GaAs layer adjacent to the nanoparticle is lower than the reference absorption without the presence of the Cu nanoparticle. The effect of the presence of Cu nanoparticle is demonstrated in Fig. 5.4.

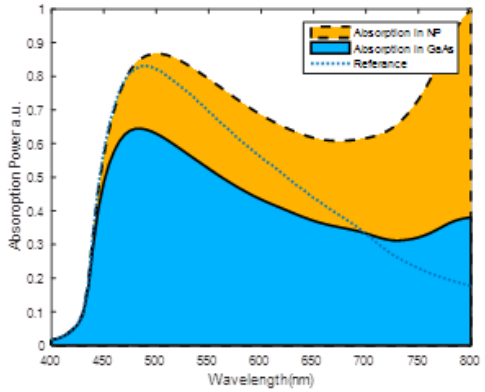

Figure 5.4: The influence on the light absorption of a 25nm radius Cu NP in the GaAs absorber layer. The dotted line is the reference absorption without the NP in the same volume of absorption

Finally, in the presence of the Aluminum (Al) nanoparticle of radius 25 nm, the GaAs absorber layer demonstrates superior absorption in much of the optical spectra. As apparent from the Fig. 5.5, the absorption in the GaAs in presence of the Al nanoparticles increases in comparison to the reference absorption for wavelengths longer than 580 nm. As evident from Fig. 5.6, for wavelengths above 580 nm the Al nanoparticle results in an absorption enhancement of up to a factor of 1.9.

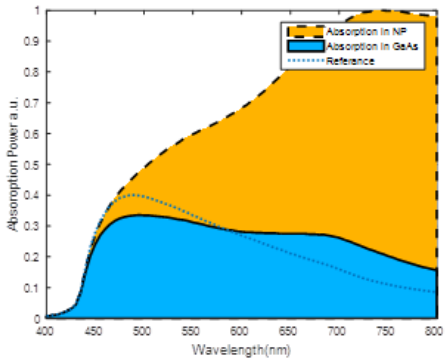

Figure 5.5: The influence on the light absorption of a 25nm radius Al NP in the GaAs absorber layer. The dotted line is the reference absorption without the NP in the same volume of absorption.

5.4 Comparison of Absorption Enhancement

The absorption enhancement for different metallic nanoparticles are illustrated in the Fig. 5.6. The maximum absorption enhancement for Ag and Cu reaches near 2.2 for the wavelength range of 400-800 nm. In contrast, even though Al nanoparticles have a lower maximum enhancement of 1.90, it has higher average enhancements in broader spectral range (600-800 nm).

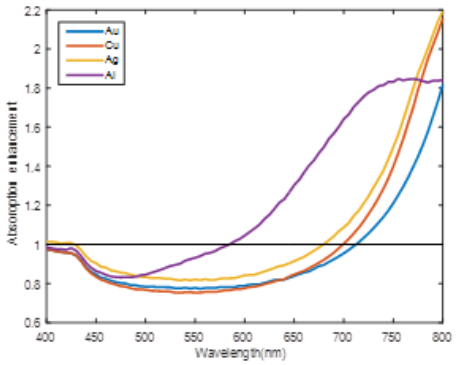

Figure 5.6 Comparison of absorption enhancement induced by the near-field of Au, Ag, Cu and Al metal nanospeheres in the GaAs absorber layer.

The average absorption enhancement in case of Al nanoparticles is 1.56 in the spectral range of 600-800 nm, which is more than that of Ag, Cu and Au with enhancements of 1.25, 1.17 and 1.07 respectively. For Au nanoparticles both the maximum enhancement and the average enhancement in the region of interest is lower than those of Ag, Cu and Al.

5.5 Effects of Size of Nanoparticles

The size of the nanoparticles play a vital role in the absorption enhancement of the GaAs absorber layer. In general, with increasing particle size the plasmon resonance peak of a plasmonic nanoparticle broadens and shifts towards higher wavelengths [126]. As Aluminum (Al) nanoparticles seem to show comparatively better performance in GaAs absorber, the results obtained from the simulation of Al nanoparticles of varying sizes in GaAs layer is presented in Fig. 5.7 for the spectral range of 400-830 nm. For a particle radius of 10nm, the maximum absorption enhancement of 1.61 is found to be around wavelength 595nm, and the absorption enhancement remains above 1, for the range of 475 to 830 nm. The highest maximum absorption enhancement of 2.08 is observed for Al particles of radius 20nm at the wavelength of 710nm and the enhancement remains above 1 for the wavelength range 535-830nm.

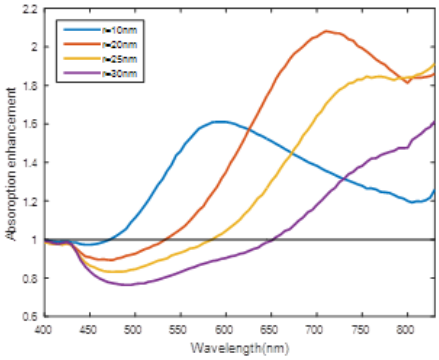

Figure 5.7: Comparison of Absorption Enhancement in GaAs for Al nanaoparticles of different radius.

A larger particle radius of 25 nm results in a bit lower maximum absorption enhancement of 1.9. The enhancement maintains a value above 1 for the spectral range of 585-830 nm, which encompasses most of the optical spectral region except the deep UV range. A further increase of nanoparticle radius to 30nm results in the decrement of the peak absorption enhancement. Moreover it also maintains an enhancement value of 1.61 for a shorter spectral range of 655-830nm. The results indicate that the optimal particle radius of Al nanoparticles should be around 20nm for much of the optical range, while 10nm radius Al particles can be considered for the deep UV range for embedding in the GaAs layer.

Chapter 6

Increased efficiency inside the CdTe solar cell absorber caused by plasmonic metal nanoparticles

6.1 Introduction

In this chapter, the same kind of properties of metal nanoparticles are studied except a CdTe absorber layer is taken. We will analyze the effects of the nanoparticle on the efficiency of the absorber layer and how it enhances the incident field and thereby increases the efficiency. Since this work is focused on near field effects of plasmonic nanoparticles, simulations were used to calculate absorption in CdTe near the nanoparticle surface. When simulating the whole solar cell structure, additional effects, such as interference, can affect the simulation results. In order to distinguish plasmonic interactions from interference effects, we used simulation geometry depicted in Fig. 6.1. In this case, we only simulate a single nanoparticle and its vicinity. The plasmonic particle is surrounded with a 20 nm CdTe region, where the absorbed energy is integrated. Simulations were done with 3D mesh, with maximum size for mesh elements of 30 nm. To avoid spurious reflections from simulation boundary, a 30 nm perfectly matched layers (PML) boundary region was used.

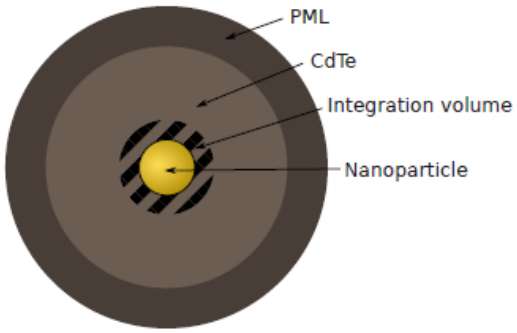

Figure 6.1: Simulation Structure with metallic NP at center surrounded by a 20nm CdTe Volume of Integration (absorption calculation made here), followed by a buffer region of GaAs of 80nm. At the boundary a 30nm PML region is present.

The PML is used to absorb propagating waves, but it is sensitive to near fields and it can cause strong distortions in simulated fields if the PML region is placed too close to the near fields. Therefore it was necessary to add an 80nm CdTe buffer region to allow the strong near fields to diminish before reaching the PML region. Commonly recommended size for the buffer region or the PML is in the order of half of the wavelength in the medium, but simulations showed that for our system the near fields of the particle decay very quickly and the large buffer layer and PML are unnecessary.

The total enhancement of absorption in the CdTe layer around an Au nanosphere can be revealed by dividing the absorption in CdTe with reference absorption. The reference absorption is calculated for CdTe volume equal to volume of the nanoparticle and surrounding integration region. By following this method we can obtain the spectral absorption enhancement.

To compare different particles, spectral absorption enhancement was averaged over wavelength range from 500 nm to 900 nm. Shorter wavelengths (below 500 nm) were outside of our interest because those wavelengths are far away from the plasmon resonance condition and there are no strong local fields. Higher wavelengths are below CdTe bandgap (1.45 eV) and therefore also outside of our interest. Optical constants for gold, silver and copper were taken from [131], for aluminium from [132], for CdTe come from Sopra N&K database and for tellurium the data is taken from [133].

6.2 Results and discussion

Overview of absorption in simulated system is shown in Fig. 6.2a. Absorption was calculated separately in the nanoparticles and in CdTe within 20 nm from the nanoparticle surface. For comparison the reference absorption is also plotted, with dashed line. The plasmon resonance peak at □ 815nm is easily recognizable. As can be seen from the figure, most of the absorption is due to the plasmonic resonance induced strong near fields in the CdTe rather than in the nanoparticle itself.

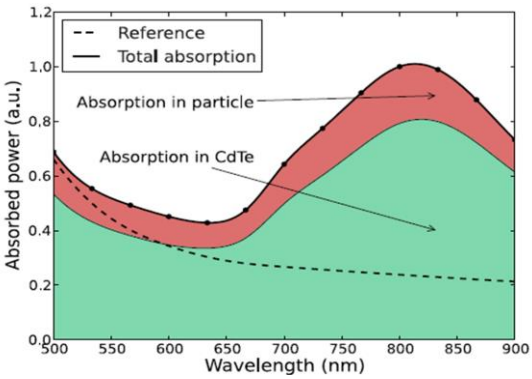

(a)

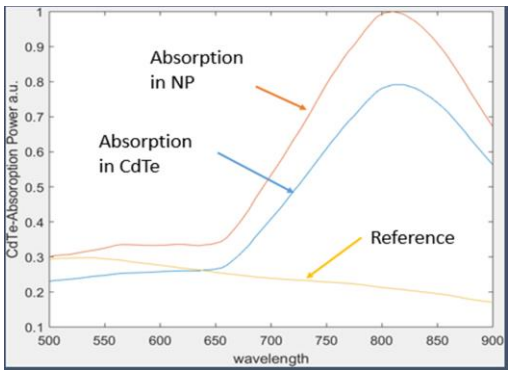

(b)

Figure 6.2: (a) Graph showing comparison of absorbed power (a.u.) in nanopartilcle and CdTe with reference absorbed power, (b) our simulation result

It is evident that for wavelengths shorter than 600nm the nanoparticles are ineffective and they are causing losses. The losses are higher in Au and Cu particles and lower in Ag particles. Greater losses in Au and Cu nanoparticles can be attributed to interband transitions in the metal. Our COMSOL simulation result in fig 6.2(b) shows deviation. This is due to taking a coarser meshing to decrease the computational load from the software which would otherwise have taken far longer time to compute the result.

The main results of this study are presented in Fig. 6.3a. Au, Ag and Cu nanoparticles all exhibit a similar behavior, having optimal particle size of about 45 nm. Aluminium particles were also simulated as these particles are sometimes used although as scattering particles [134]. Since the plasmonic resonance of the aluminium particle is outside of the interesting spectral range of 500 nm - 900 nm, there are no strong fields and associated local absorption enhancement.

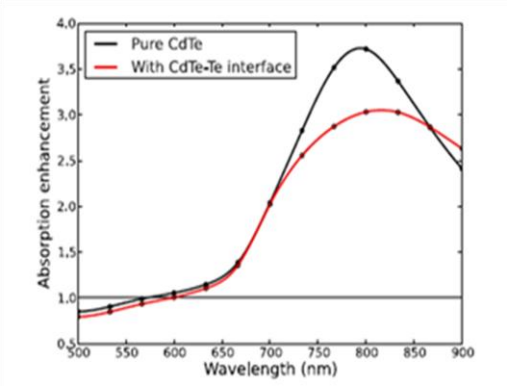

(a)

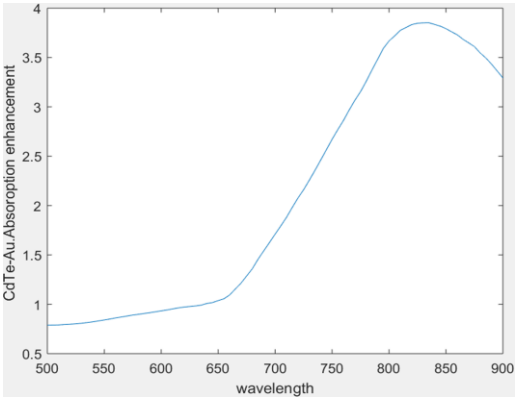

(b)

Figure 6.3: (a) Absorption enhancement comparison (b) Our simulation result

Chapter 7

Metal Nanoparticle Induced Enhancement of Light Absorption in Perovskite Solar Cells

7.1 Introduction

A perovskite solar cell incorporates perovskite structured compound, most commonly a hybrid organic-inorganic lead or tin halide-based material. Very recently, organometal halide perovskites have been employed as the absorber layer in hybrid solar cell [135, 136]. Over the last five years, silicon-based solar cells have seen a new competitor as organic photovoltaic devices, particularly the bulk heterojunction architecture, have allowed power conversion efficiencies around 8% [137]. Solar cells incorporating perovskite materials is now the fastest advancing photovoltaic (PV) technology with their efficiencies having increased from 3.8% in 2009 [138] to 22.1% in early 2016 [136]. These materials show highly enhanced low-loss photovoltaic operation in addition to a simple synthetic route which is solution based from abundant sources (C, N, Pb, and Halogen). One very commonly known perovskite-compound type, methylammonium halides, have been reported to show 3.8% increased efficiency. This CH3NH3PbI3 "perovskite sensitized" solar cell (PSSC) is constructed employing a liquid electrolyte in a dye-sensitized solar cell (DSSC) architecture [138]. It can facilitate an efficient electron transport pathway without the need for an n-type oxide, which removes a huge loss interface in the sensitized approach. Also, this material can effectively operate as a solid-thin film semi-conductor, taking up all the roles of light absorption. Furthermore, very effective transportation of electrons and holes are also observed [139]. The halide content in the material can be deemed as a bandgap controller [140]. Having a long diffusion length of over 1 micron, these materials can function effectively in a thin-film structure [141]. All these properties demonstrate that perovskites hold great potential as cheap and highly efficient absorber materials for solution processed PV cells.

Moreover, perovskite absorber layers are also able to facilitate the use of metallic nanoparticles (NP) for increasing the performance of the solar cell, although the exact physical mechanism behind such improvement is still to be properly explored [142]. There is versatility in ways the metallic NP can be incorporated into solar cells. Light absorption cross-sectional area can be increased by enhancing the local electric field of metal NPs upon surface plasmon resonance [142-145]. Again manipulative light scattering property can be used to redirect light into solar cell increasing the optical path-length [146]. Metal NP can also be utilized as a sensitizer directly, to harness light and inject photon-induced electrons to an electron acceptor [147]. This study concentrates on the effects of the near-field enhancements of the metal nanoparticles (NP) on the Methylammonium Lead Iodide ($CH_3NH_3PbI_3$)

Perovskite absorber layer. To the best of our knowledge this is the first work that computationally investigates the enhancement of light absorption efficiency in Perovskite absorber layer due to the embedding of metal nanoparticles. A large portion of the solar spectrum is absorbed poorly by thin film solar cells, especially in the intense 600

1100 nm region [148]. Thus, the impact of metal nanoparticles of Gold (Au) and Silver (Ag) were studied using the finite element computer simulation software COMSOL Multiphysics and the absorption of Perovskite in each case was compared, in the 400-900 nm spectral range. The light absorption and its enhancement is also dependent on the size of the nanoparticles inside the absorber layer. Varying the radius of the embedded nanoparticles, their effects on light absorption on the Perovskite absorber layer were also studied.

7.2 Simulation Settings

For the nanoparticles, the scattered field formulation was solved by the finite element method simulation software COMSOL Multiphysics 5.2. As this work was primarily concerned with the near field effects of plasmonic nanoparticles, simulations were performed to calculate the absorption in Perovskite near the nanoparticle surface. While simulating the whole solar cell structure, unwanted additional effects, e.g. interference may affect the simulation. To avert this problem and calculate the plasmonic interaction in the near field of the metal NPs, and differentiate it from effects superfluous to our study, the 3D simulation geometry is used as depicted in Fig. 7.1. The total energy absorbed G_v by the Perovskite absorber was calculated by integrating the absorption in a 20nm Perovskite layer of volume V, adjacent to the metallic nanoparticle. This was performed by calculating the total electromagnetic power loss Q_e in Perovskite absorber layer, modeled as

$$G_v = \int_v Q_e dv \tag{7.1}$$

across the 400-900 nm range. A mesh size of maximum 30 nm was used.

Along the boundary of the simulation space, a perfectly matched layer (PML) of 30nm was set up. The prime function of the PML is to strongly absorb the outward propagating electromagnetic waves from the interior of a computational region without reflecting them back. A space of about 80nm of Perovskite was kept between the PML and the integrating volume V of interest so that the strong near fields may fully diminish before interacting with the PML which might cause severe distortions [149].

To observe the absorption enhancement Abs_e, the absorption in the integrating volume of Perovskite surrounding the nanoparticle was divided by the reference absorption G_{ref} of the Perovskite without the presence of the nanoparticle.

$$Abs_e = \frac{\int_v Q_e dv}{G_{ref}} \tag{7.2}$$

Where the reference absorption G_{ref} is calculated as:

$$G_{ref} = \int_v Q_{np} dv + \int_v Q_{ve} dv \tag{7.3}$$

Integrating the total absorption in the integrating volume of interest Q_{ve} and the absorption in the nanoparticle volume Q_{np} without the presence of any foreign metallic nanoparticle. The wavelength range of 400 nm to 900 nm was included in the work because the Perovskite has a bandgap of 1.55 eV (which corresponds to 800nm) [150]. The optical constants of gold and silver were taken from [151] and optical constants of Perovskite layer from [152].

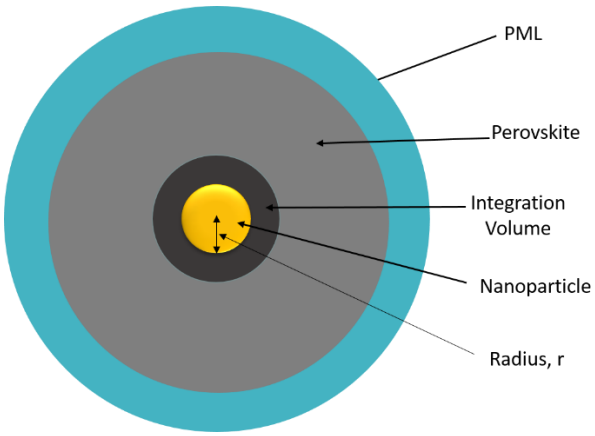

Figure 7.1: Simulation Structure with metallic NP at center surrounded by a 20nm Perovskite Volume of Integration (absorption calculation made here), followed by a buffer region of Perovskite of 80nm. At the boundary a 30nm PML region is present.

7.3 Comparison of Metal Nanoparticles

An enhancement of absorption occurs when the absorption in the presence of a metallic nanoparticle within the perovskite volume of interest G_v is larger than the reference absorption G_{ref}. For an Au

nanoparticle of radius 25 nm, the absorption in the Perovskite absorber layer with and without the presence of the nanoparticle is illustrated in the Fig. 7.2.

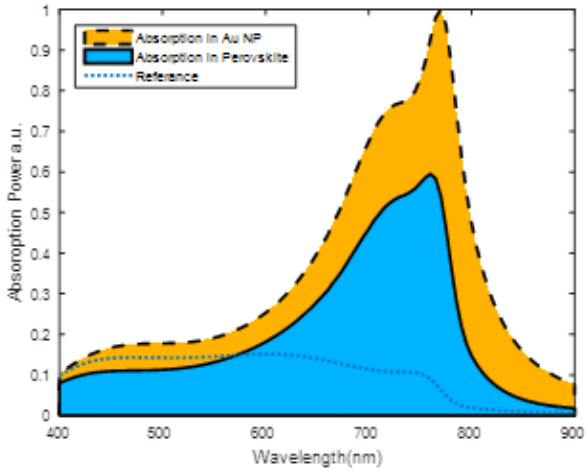

Figure 7.2: The influence of a 25nm radius Au NP on the light absorption with in the Perovskite absorber layer. The dotted line is the reference absorption without the NP in the same volume of absorption

The yellow and blue colored area corresponds respectively to the absorption in the nanoparticle and the absorption in the perovskite layer adjacent to the nanoparticle which were independently determined. The reference absorption is also indicated in dotted lines for comparison. For wavelength higher than 575 nm, Au nanoparticle is effective in the absorber media as the reference absorption of Perovskite is lower than that with the presence of Au nanoparticles in this spectral range. This can be perceived clearly from the absorption enhancement in Fig. 7.6.

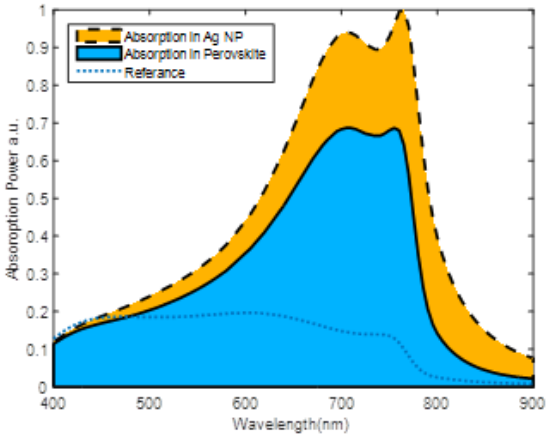

Figure 7.3: The influence on the light absorption of a 25nm radius Ag NP in the Perovskite absorber layer. The dotted line is the reference absorption without the NP in the same volume of absorption

From Fig. 3 it is evident that, for Ag NP effective range starts from 575nm as well, while a shift can be seen in effective range starting from 480nm for Cu in Fig. 7.5.

NP	Maximum enhancement	Wavelength (nm) of maximum enhancement	Average enhancement Range
Au	9.62	780nm	4.30
Ag	7.09	775nm	4.04
Al	1.74	665nm	1.68
Cu	7.12	775nm	3.71

Table 7.1

For Al NP (Fig. 7.4) almost whole spectrum, starting from 425nm proves to be effective in absorber media.

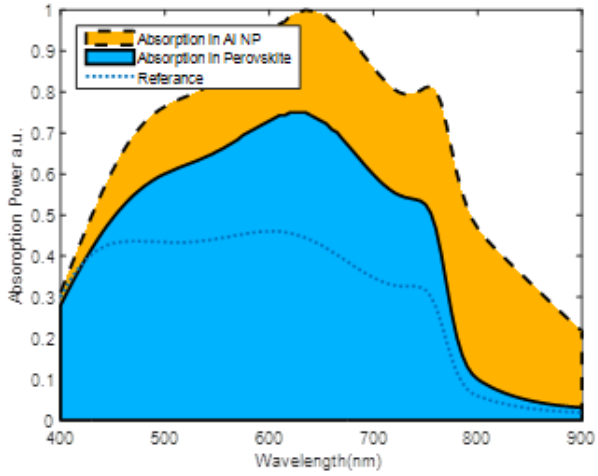

Figure 7.4: The influence on the light absorption of a 25nm radius Al NP in the Perovskite absorber layer. The dotted line is the reference absorption without the NP in the same volume of absorption.

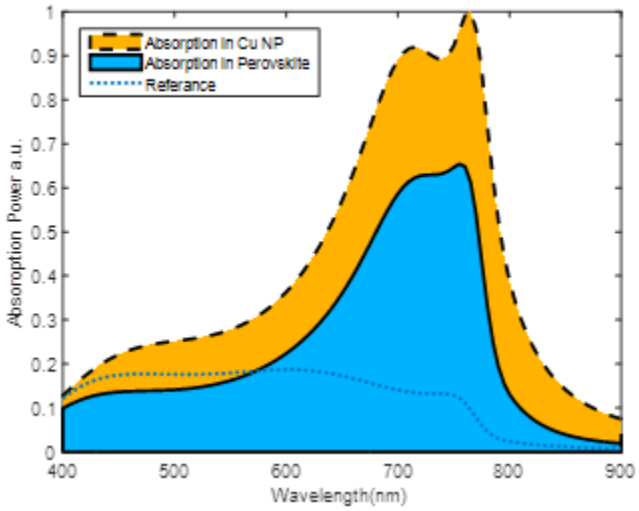

Figure 7.5: The influence on the light absorption of a 25nm radius Cu NP in the Perovskite absorber layer. The dotted line is the reference absorption without the NP in the same volume of absorption.

7.4 Comparison of Absorption Enhancement

The absorption enhancement for Au (gold), Ag (silver), Al (aluminum) & Cu (copper) nanoparticles are illustrated in the Fig. 7.6. While we can see Au, Ag & Cu showing a pattern, Al happened to enhance almost all over the spectrum starting from 425nm. A comparison of absorption enhancement due the NPs is shown in Table-I. For average enhancement calculation, we measure the enhancement in near the infrared region starting from wavelength 600nm to 900nm. Change in absorption enhancement along the wavelength range for Au, Ag, Al, Cu NPs at 25nm radius is shown in Fig. 7.6.

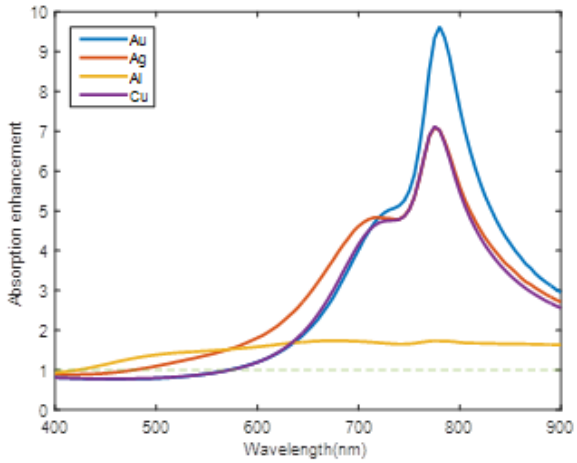

Figure 7.6: Comparison of absorption enhancement induced by the near-field of Au, Ag, Al, Cu metal nanospeheres in the Perovskite absorber layer.

7.5 Effects of Size of Nanoparticles

The size of the nanoparticles plays a vital role in the absorption enhancement of the Perovskite absorber layer. In general, with increasing particle size the plasmon resonance peak of a plasmonic nanoparticle broadens and shifts towards higher wavelengths [152-155]. Further investigation is done by varying all the NP sizes & results in shown in Fig. 7.5. The enhancement increment with changing radius is shown in the Table-II where maximum enhancement if measured for wavelength range of 400-900 nm and average enhancement is measured for the range of 600-900 nm as enhancement most likely to be above 1 in this range observed from Fig 7.6.

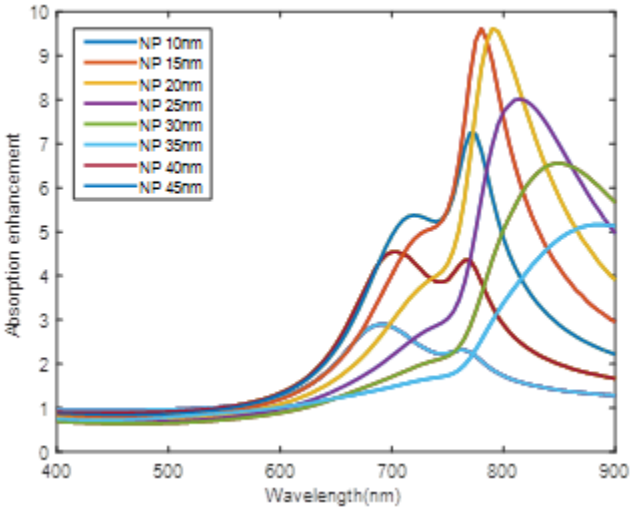

Figure 7.7: Comparison of Absorption Enhancement in Perovskite for Au nanaoparticles of different radius.

NP radius	Maximum enhancement	Wavelength(nm) of maximum enhancement	Average enhancement range
10nm	2.90	690nm	1.91
15nm	4.53	700nm	2.88
20nm	7.25	770nm	3.76
25nm	9.62	780nm	4.30
30nm	9.62	790nm	4.37
35nm	8.01	815nm	3.99
40nm	6.55	850nm	3.30
45nm	5.16	885nm	2.61

Table 7.2

From Fig.7.7 it is evident that, as the radius of Au NP increases, maximum absorption enhancement reaches a value of 9.62 at wavelength 780nm for a NP of radius 25nm. The same amount of absorption enhancement is obtained at the presence of 30nm Au NP but with a slight shift of wavelength, at 790nm

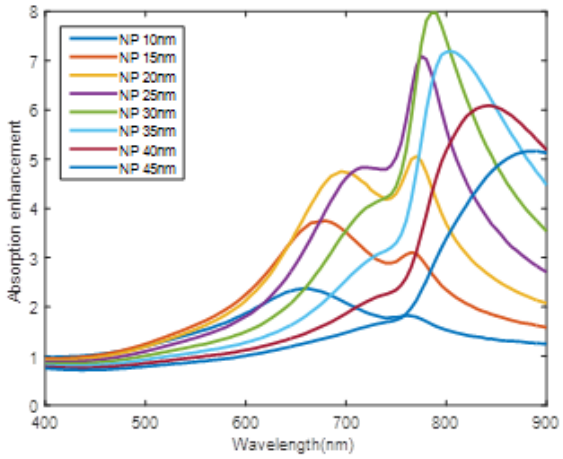

Figure 7.8: Comparison of Absorption Enhancement in Perovskite for Ag nanaoparticles of different radius.

with a slightly higher absorption enhancement of 4.37. Above 30nm, as the radius is increased, a decline is noticed in maximum absorption enhancement. The details are summarized on Table-II.

NP radius	Maximum enhancement	Wavelength(nm) of maximum enhancement	Average enhancement
10nm	2.38	660nm	1.78
15nm	3.75	780nm	2.69
20nm	5.06	770nm	3.50
25nm	7.09	775nm	4.04
30nm	7.97	790nm	4.18
35nm	7.19	805nm	3.90
40nm	6.08	840nm	3.31
45nm	5.15	890nm	2.61

Table 7.3

While using Ag as NP, maximum absorption enhancement of 7.97 is obtained in absorber layer at the wavelength of 790nm for 30nm radius NP & from Fig. 7.8 it is observed that beyond a NP radius of 30nm

the absorption enhancement starts to decrease. Details of absorption enhancement for Ag NP provided in Table-III.

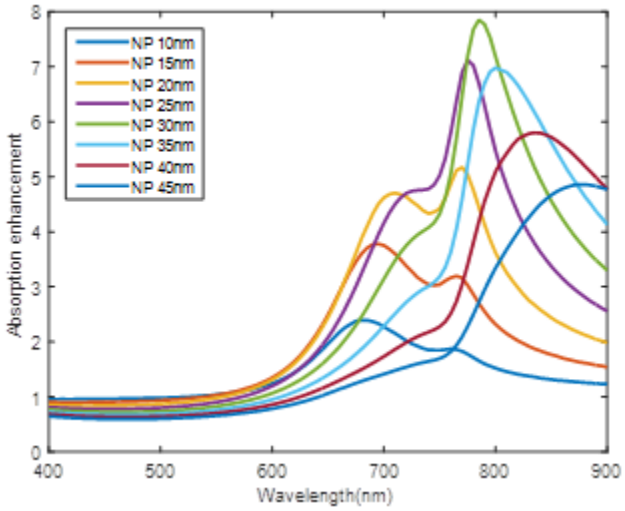

Figure 7.9: Comparison of Absorption Enhancement in Perovskite for Cu nanaoparticles of different radius.

NP radius	Maximum enhancement	Wavelength(nm) of maximum enhancement	Average enhancement
10nm	2.40	680nm	1.69
15nm	3.78	695nm	2.46
20nm	5.17	770nm	3.21
25nm	7.11	775nm	3.71
30nm	7.85	785nm	3.86
35nm	6.97	800nm	3.63
40nm	5.80	835nm	3.11
45nm	4.86	880nm	2.48

Table 7.4

Almost similar result is achieved with a lower maximum absorption enhancement of 7.85 at wavelength 785nm when Cu is used as NP in the perovskite absorber layer as inferred from Fig. 7.9. Absorption enhancement starts to decline as the radius of Cu NP is increased. The variations in absorption enhancement due to change of Cu radius are delineated in Table-IV.

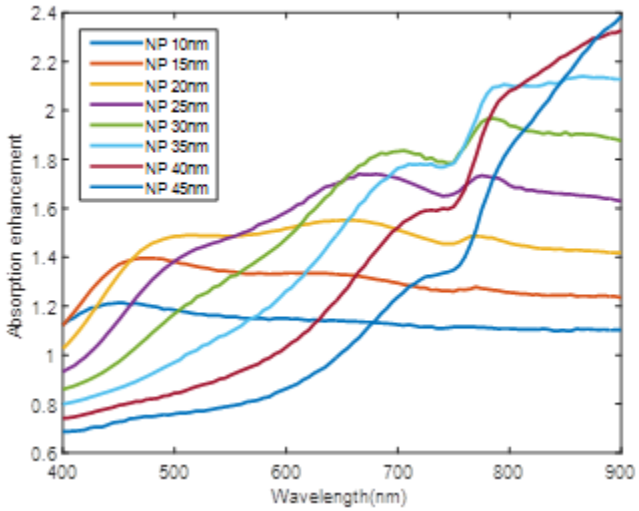

Figure 7.10: Comparison of Absorption Enhancement in Perovskite for Al nanaoparticles of different radius

NP radius	Maximum enhancement	Wavelength(nm) of maximum enhancement	Average enhancement
10nm	1.21	450nm	1.12
15nm	1.40	470nm	1.28
20nm	1.55	650nm	1.48
25nm	1.74	665nm	1.68
30nm	1.97	785nm	1.81
35nm	2.14	865nm	1.82
40nm	2.33	900nm	1.72
45nm	2.38	900nm	1.52

Table 7.5

On the other hand, in Fig. 7.10 Al demonstrates somewhat different characteristics when it was used as NP in the perovskite absorber layer. It shows almost even absorption enhancement throughout the wavelength range with maximum enhancement of 2.38 nm for 45nm radius Al NP in the 900nm wavelength, but within the bandgap wavelength of perovskite the maximum absorption enhancement is 2.2 for 40 nm radius of Al NP. As evident from the Table- V, the average enhancement of maximum 1.82 is present for 40 nm radius Al NP and beyond this it decreases as the NP radius is increased.

Chapter 8

Conclusion

8.1 Summary

Physically thin but optically thick photovoltaic absorbers has the potential to transform high-efficiency and low cost solar cell designs. This can be achieved by light trapping utilizing the resonant scattering and concentration of light by exploiting metallic nanoparticles. We have investigated the enhancement of light absorption in the GaAs layer due to the influence of strong near fields caused by plasmonic nanoparticles. The results concluded that absorption enhancement up to a factor of ~2 is possible in the GaAs absorber layer, by the aid of metallic nanoparticles in the 600-800 nm range, where in general thin film solar cells have poor absorption. The absorption enhancement in the instance of Al nanoparticle is significant in a broader optical range compared to Au, Ag and Cu. According to the results employing Al nanoparticles of radius 20nm ensures the best performance among the considered metal nanoparticles. This simulation suggests the possibility of using Aluminum nanoparticles for enhanced efficiencies and light absorption in GaAs thin-film solar cells. We also investigated influence of strong near fields caused by plasmonic nanoparticles to the absorption in the CdTe layer. It was found that the spectrally averaged absorption enhancement can be locally enhanced up to 2.5 times in the vicinity of noble metal nanoparticle. Particularly silver or gold nanoparticle with diameters 45-50 nm provided theoretical enhancement of light absorption in the range 650-900 nm with maximum at 815 nm. According to our calculations, interaction of plasmons induced in neighboring nanoparticles become significant only at quite small distances ≤ 50 nm between them. It will allow essential doping of CdTe material by nanoparticles without strong broadening or red shifting of plasmon resonance spectral band.

Perovskite solar cells have the potential to transform high-efficiency and low cost solar cell designs. This can further be boosted by light trapping, utilizing the resonant scattering and concentration of light by exploiting metallic nanoparticles. We have computationally investigated for the first time (to the best of our knowledge) the enhancement of light absorption on the Methylammonium Lead Iodide ($CH_3NH_3PbI_3$) Perovskite absorber layer due to the influence of strong near fields caused by Au & Ag nanoparticles. The results concluded that absorption enhancement up to a factor of 9.62 is possible using 25nm & 30nm Au NP in the Perovskite absorber layer, by the aid of metallic nanoparticles in the 400-900 nm spectral range, where in general thin film solar cells have poor absorption. The absorption enhancement in the instance of Au nanoparticle is significant in a broader optical range compared to Ag. According to the results employing Au nanoparticles of radius 35 nm ensures the best performance among the considered metal nanoparticles. This simulation suggests the possibility of using Au nanoparticles for enhanced light absorption in perovskite solar cells.

8.2 Future Works

Our future goal is to use dimetal as nanoparticles in the absorber layer of a solar cell. As explained in chapter 4 dimer shells show resonance peak (hot spot) with a particular separation distance in air. We would like to implement this phenomenon in the absorber layer of a solar cell. Also the accommodation of an array of metal nanoparticles fine-tuned in separation distance and radius to bring out the maximum possible enhancement in absorption for a particular frequency. Furthermore 2D materials like graphene is showing huge promise as absorber layer. We would also try out different metamaterials and examine their plasmonic properties and how they tie in to solar cells.

References

[1] N. S. Lewis. "Powering the planet". *MRS Bulletin*, 2007.

[2] A. Luque and S. Hegedus. "Handbook of Photovoltaic Science and Engineering". *John Wiley & Sons*, England, 2003.

[3] M. A. Green. "Third generation photovoltaics: solar cells for 2020 and beyond". *Physica E-Low-Dimensional Systems & Nanostructures*, 14(1-2):65{70, 2002.

[4] A. Romeo, A. Terheggen, D. Abou-Ras, D. L. Batzner, F. J. Haug, M. Kalin, D. Rudmann, and A. N. Tiwari. "Development of thin-film Cu(In,Ga)Se-2 and CdTe solar cells". *Progress in Photovoltaics*, 12(2-3):93-111, 2004.

[5] M. A. Contreras, B. Egaas, K. Ramanathan, J. Hiltner, A. Swartzlander, F. Hasoon, and R. Nou. "Progress toward 20% efficiency in Cu (In,Ca)Se-2 polycrystalline thin-film solar cells". *Progress in Photovoltaics*, 7(4):311-316, 1999.

[6] G. Mie. "Beitrage zur optik truber medien, speziell kolloidaler metal osungen. Annalen Der Physik", 25(3):377{445, 1908.

[7] R. H. Ritchie. "Plasma losses by fast electrons in thin films". *Physical Review*, 106, 1957.

[8] A. Otto. "Exictation of Nonradiative Surface Plasma Waves in Silver by Method of Frustrated Total Reection". *Zeitschrift fur Physik*, 216(4):398 &, 1968.

[9] E. Kretschmann and H. Raether. "Radiative decay of non-radiative surface plasmons excited by light". *Zeitschrift fur Naturforschung*, 23A, 1968.

[10] D. L. Jeanmaire and R. P. Van Duyne. "Surface raman spectroelectrochemistry: Part i. heterocyclic, aromatic, and aliphatic amines adsorbed on the anodized silver electrode". *Journal of Electroanalytical Chemistry*, 84:1{20, 1977.

[11] K. A. Willets and R. P. Van Duyne. "Localized surface plasmon resonance spectroscopy and sensing". *Annual Review of Physical Chemistry*, 58:267{297, 2007.

[12] A. Polman. "Applied Physics Plasmonics Applied. Science", 322(5903):868{869, 2008.

[13] J. Mertz. "Radiative absorption, fluorescence, and scattering of a classical dipole near a lossless interface: a unfied description". *Journal of the Optical Society of America B-Optical Physics*, 17(11):1906{1913, 2000.

[14] J. B. Pendry. "Negative refraction makes a perfect lens". *Physical Review Letters*, 85(18):3966-3969, 2000.

[15] R. J. Walters, R. V. A. van Loon, I. Brunets, J. Schmitz, and A. Polman. "A silicon-based electrical source of surface plasmon polaritons". *Nature Materials*, 9(1):21-25, 2010.

[16] R. F. Oulton, V. J. Sorger, T. Zentgraf, R.-M. Ma, C. Gladden, L. Dai, G. Bartal, and X. Zhang. "Plasmon lasers at deep subwavelength scale". *Nature*, 461 (7264):629{632, 2009.

[17] M. T. Hill, Y.-S. Oei, B. Smalbrugge, Y. Zhu, T. De Vries, P. J. Van Veldhoven, F. W. M. Van Otten, T. J. Eijkemans, J. P. Turkiewicz, H. De Waardt, E. J. Geluk, S.-H. Kwon, Y.-H. Lee, R. Notzel, and M. K. Smit. "Lasing in metallic- Coated nanocavities". *Nature Photonics*, 1(10):589-594, 2007.

[18] S. Lal, S. E. Clare, and N. J. Halas. "Nanoshell-Enabled Photothermal Cancer Therapy: Impending Clinical Impact". *Accounts of Chemical Research*, 41(12, Sp. Iss. SI) :1842-1851, 2008.

[19] S. Pillai, K. R. Catchpole, T. Trupke, and M. A. Green. "Surface plasmon enhanced silicon solar cells". *Journal of Applied Physics*, 101(9), 2007.

[20] D. Derkacs, S. H. Lim, P. Matheu, W. Mar, and E. T. Yu. "Improved performance of amorphous silicon solar cells via scattering from surface plasmon polaritons in nearby metallic nanoparticles". *Applied Physics Letters*, 89(9), 2006.

[21] K. Nakayama, K. Tanabe, and H. A. Atwater. "Plasmonic nanoparticle enhanced light absorption in GaAs solar cells". *Applied Physics Letters*, 93(12), 2008.

[22] R. B. Konda, R. Mundle, H. Mustafa, O. Bamiduro, A. K. Pradhana, U. N. Roy, Y. Cui, and A. Burger. "Surface plasmon excitation via Au nanoparticles in n-CdSe/p-Si heterojunction diodes". *Applied Physics Letters*, 91(19), 2007.

[23] I. M. Pryce, D. D. Koleske, A. J. Fischer, and H. A. Atwater. "Plasmonic nanoparticle enhanced photocurrent in GaN/InGaN/GaN quantum well solar cells". *Applied Physics Letters*, 96(15), 2010.

[24] D. Derkacs, W. V. Chen, P. M. Matheu, S. H. Lim, P. K. L. Yu, and E. T. Yu. "Nanoparticle-induced light scattering for improved performance of quantumwell solar cells". *Applied Physics Letters*, 93(9), 2008.

[25] A. J. Morfa, K. L. Rowlen, T. H. Reilly, III, M. J. Romero, and J. van de Lagemaat. "Plasmon-enhanced solar energy conversion in organic bulk heterojunction photovoltaics". *Applied Physics Letters*, 92(1), 2008.

[26] M. Westphalen, U. Kreibig, J. Rostalski, H. Luth, and D. Meissner. "Metal cluster enhanced organic solar cells". *Solar Energy Materials and Solar Cells*, 61 (1):97-105, 2000.

[27] C. Wen, K. Ishikawa, M. Kishima, and K. Yamada. "Effects of silver particles on the photovoltaic properties of dye-sensitized TiO2 thin films". *Solar Energy Materials and Solar Cells*, 61(4):339-351, 2000.

[28] Tanabe, K. (2009). "A Review of Ultrahigh Efficiency III-V Semiconductor Compound Solar Cells: Multijunction Tandem, Lower Dimensional, Photonic Up/Down Conversion and Plasmonic Nanometallic Structures".

[29] P. Spinelli, M. Hebbink, R. de Waele, L. Black, F. Lenzmann, and A. Polman. "Optical impedance matching using coupled plasmonic nanoparticle arrays". *Nano Letters*, 11(4):1760-1765, 2011.

[30] J. N. Munday and H. A. Atwater. "Large integrated absorption enhancement in plasmonic solar cells by combining metallic gratings and antireection coatings". *Nano Letters*, 2011.

[31] Ferry, Vivian E.; Sweatlock, Luke A.; Pacifici, Domenico; Atwater, Harry A. (2008). "Plasmonic Nanostructure Design for Efficient Light Coupling into Solar Cells". *Nano Letters*.

[32] Vincenzo Giannini, Antonio I. Fernandez-Domínguez, Susannah C. Heck, and Stefan A. Maier. "Plasmonic Nanoantennas: Fundamentals and Their Use in Controlling the Radiative Properties of Nanoemitters" .2010

[33] A. Garc´ıa-Etxarri, R. G´omez-Medina, L. S. Froufe-P´erez, C. L´opez,2 L. Chantada, F. Scheffold, J. Aizpurua, M. Nieto-Vesperinas, and J. J. S´aenz, "Strong magnetic response of submicron Silicon particles in the infrared" .2010

[34] P. Colomban, G. March, L. Mazerolles, T. Karmous, N. Ayed, A. Ennabli, and H. Slim. "Raman identification of materials used for jewellery and mosaics". J. Raman Spectrosc., 34:205, 2003.

[35] Katja Ehrhold, Silke Christiansen, and Ulrich Gosele. "Plasmonic Properties of Bimetal Nanoshell Cylinders and Spheres" 2009

[36] Y. Ekinci, H. H. Solak, and J. F. Löffler "Plasmon resonances of aluminum nanoparticles"

[37] T. Repäna, S. Pikkera, L. Dolgova, A. Loota, J. Hiieb, M. Krunksb, I. Sildosa. "Increased efficiency inside the CdTe solar cell absorber caused by plasmonic metal nanoparticles". 2008

[38] N. P. Hylton, X. F. Li, V. Giannini, K. H. Lee, N. J. Ekins-Daukes, J. Loo, D. Vercruysse, P. Van Dorpe, H. Sodabanlu5, M. Sugiyama & S. A. Maier. "Loss mitigation in plasmonic solar cells aluminium nanoparticles for broadband photocurrent enhancements in GaAs photodiodes". 2009

[39] Qian Zhou, Debao Jiao, Kailiang Fu, Xiaojie Wua, Yongsheng Chen a, Jingxiao Lu a, Shi-e Yang. "Two-dimensional device modeling of CH3NH3PbI3 based planar heterojunction perovskite solar cells" 2009.

[40] Wei Zhang, Michael Saliba, Samuel D. Stranks, Yao Sun, Xian Shi,‡ Ulrich Wiesner, and Henry J. Snaith. "Enhancement of Perovskite-Based Solar Cells Employing Core−Shell Metal Nanoparticles".

[41] I. Nakai, C. Numako, H. Hosono, and K. Yamasaki. "Origin of the red color of Satsuma copper-ruby glass as determined by EXAFS and optical absorption spectroscopy". *J. Am. Ceram. Soc*., 82:689, 1999.

[42] P. Colomban. "The use of metal nanoparticles to produce yellow, red and iridescent colour, from Bronze Age to present times in lustre pottery and glass: Solid state chemistry, spectroscopy and nanostructure". J. Nano Res., 8:109, 2009.

[43] F. Hallermann, C. Rockstuhl, S. Fahr, G. Seifert, S.Wackerow, H. Graener, G. v. Plessen, and F. Lederer. "On the use of localized plasmon polaritons in solar cells". Phys. Status Solidi A, 205:2844, 2008.

[44] P. Spinelli, V. E. Ferry, J. van de Groep, M. van Lare, M. A. Verschuuren, R. E. I. Schropp, H. A. Atwater, and A. Polman. "Plasmonic light trapping in thin-film Si solar cells". J. Opt., 14:024002, 2012.

[45] S. B. Mallick, N. P. Sergeant, M. Agrawal, J.-Y. Lee, and P. Peumans. "Coherent light trapping in thin-film photovoltaics". MRS Bulletin, 36:453, 2011.

[46] S. A. Choulis, M. K. Mathai, and V.-E. Choong. "Influence of metallic nanoparticles on the performance of organic electrophosphorescence devices". Appl. Phys. Lett., 88:213503, 2006.

[47] A. Fujiki, T. Uemura, N. Zettsu, M. Akai-Kasaya, A. Saito, and Y. Kuwahara. "Enhanced fluorescence by surface plasmon coupling of au nanoparticles in an organic electroluminescence diode". Appl. Phys. Lett., 96:043307, 2010.

[48] C. Huh, C.-J. Choi, W. Kim, B. K. Kim, B.-J. Park, E.-H. Jang, S.-H. Kim, and G. Y. Sung. "Enhancement in light emission efficiency of Si nanocrystal light-emitting diodes by a surface plasmon coupling". Appl. Phys. Lett., 100:181108, 2012.

[49] K. M. Mayer and J. H. Hafner. "Localized surface plasmon resonance sensors". Chem. Rev., 111:3828, 2011.

[50] H. Haick. "Chemical sensors based on molecularly modified metallic nanoparticles". J. Phys. D: Appl. Phys., 40:7173, 2007.

[51] M. De, P. S. Ghosh, and V. M. Rotello. "Applications of nanoparticles in biology". *Adv. Mater*., 20:4225, 2008.

[52] S. Schlücker. 'SERS microscopy: nanoparticle probes and biomedical applications". ChemPhysChem, 10:1344, 2009.

[53] X. X. Han, B. Zhao, and Y. Ozaki. "Surface-enhanced Raman scattering for protein detection". Anal. Bioanal. Chem., 394:1719, 2009.

[54] K. Mori, M. Kawashima, M. Che, and H. Yamashita. "Enhancement of the photoinduced oxidation activity of a ruthenium (ii) complex anchored on silica-coated silver nanoparticles by localized surface plasmon resonance". Angew. Chem. Int. Ed. Engl., 49:8598, 2010.

[55] S. Kéna-Cohen, A. Wiener, Y. Sivan, P. N. Stavrinou, D. D. C. Bradley, A. Horsfield, and S. A. Maier. "Plasmonic sinks for the selective removal of long-lived states". *ACS Nano*, 5:9958, 2011.

[56] Bjoern NIESEN. "Performance improvement of organic solar cells by metallic nanoparticles". 2011

[57] M. A. Noginov, G. Zhu, A. M. Belgrave, R. Bakker, V. M. Shalaev, E. E. Narimanov, S. Stout, E. Herz, T. Suteewong, and U. Wiesner. "Demonstration of a spaser-based nanolaser". *Nature*, 460:1110, 2009.

[58] E. Cubukcu, E. A. Kort, K. B. Crozier, and F. Capasso. "Plasmonic laser antenna". *Appl. Phys. Lett.*, 89:093120, 2006.

[59] S. A. Maier. "Plasmonics: fundamentals and applications". Springer Science+Business Media, New York, 2007.

[60] U. Kreibig and M. Vollmer. "Optical properties of metal clusters". *Springer: Berlin*, 1995.

[61] M. A. Garcia. "Surface plasmons in metallic nanoparticles: fundamentals and applications". *J. Phys. D: Appl. Phys.*, 44:283001, 2011.

[62] P. Zijlstra and M. Orrit. "Single metal nanoparticles: optical detection, spectroscopy and applications". *Rep. Prog. Phys.*, 74:106401, 2011.

[63] V. Giannini, A. I. Fernandez-Dominguez, S. C. Heck, and S. A. Maier. "Plasmonic nanoantennas: Fundamentals and their use in controlling the radiative properties of nanoemitters". *Chem. Rev.*, 111:3888, 2011.

[64] A. V. Zayats, I. I. Smolyaninov, and A. A. Maradudin. "Nano-optics of surface plasmon polaritons". *Phys. Rep.,* 408:131, 2005.

[65] J. M. Pitarke, V. M. Silkin, E. V. Chulkov, and P. M. Echenique. "Theory of surface plasmons and surface-plasmon polaritons". *Rep. Prog. Phys.*, 70:1, 2007.

[66] A. V. Zayats and I. I. Smolyaninov. "Near-field photonics: surface plasmon polaritons and localized surface plasmons". *J. Opt. A: Pure Appl. Opt.*, 5:S16, 2003.

[67] J. Prikulis, P. Hanarp, L. Olofsson, D. Sutherland, and M. Käll. "Optical spectroscopy of nanometric holes in thin gold films". *Nano Lett.*, 4:1003, 2004.

[68] J. Parsons, E. Hendry, C. P. Burrows, B. Auguie, J. R. Sambles, and W. L. Barnes." Localized surface-plasmon resonances in periodic nondiffracting metallic nanoparticle and nanohole arrays". *Phys. Rev. B*, 79:073412, 2009.

[69] A. I. Henry, J. M. Bingham, E. Ringe, L. D. Marks, G. C. Schatz, and R. P. Van Duyne. "Correlated structure and optical property studies of plasmonic nanoparticles'. *J. Phys. Chem. C*, 115:9291, 2011.

[70] M. Rycenga, C. M. Cobley, J. Zeng, W. Li, C. H. Moran, Q. Zhang, D. Qin, and Y. Xia. "Controlling the synthesis and assembly of silver nanostructures for plasmonic applications". *Chem. Rev.*, 111:3669, 2011.

[71] A. Tcherniak, J. W. Ha, S. Dominguez-Medina, L. S. Slaughter, and S. Link. "Probing a century old prediction one plasmonic particle at a time". *Nano Lett.*, 10:1398, 2010.

[72] C. Noguez. "Surface plasmons on metal nanoparticles: The influence of shape and physical environment". *J. Phys. Chem*. C, 111:3806, 2007.

[73] P. K. Jain, K. S. Lee, I. H. El-Sayed, and M. A. El-Sayed. "Calculated absorption and scattering properties of gold nanoparticles of different size, shape, and composition: applications in biological imaging and biomedicine". *J. Phys. Chem. B*, 110:7238, 2006.

[74] O. Muskens, P. Billaud, M. Broyer, N. Del Fatti, and F. Vallée. "Optical extinction spectrum of a single metal nanoparticle: Quantitative characterization of a particle and of its local environment". *Phys. Rev. B*, 78:205410, 2008.

[75] M. M. Miller and A. A. Lazarides. "Sensitivity of metal nanoparticle plasmon resonance band position to the dielectric environment as observed in scattering". *J. Opt. A-Pure Appl. Opt.*, 8:S239, 2006.

[76] M. Meier and A. Wokaun. "Enhanced fields on large metal particles: dynamic depolarization". *Opt. Lett.*, 8:581, 1983.

[77] C. F. Bohren and D. R. Huffman. "Absorption and scattering of light by small particles". *Wiley Interscience*: New York, 1983.

[78] K. L. Kelly, E. Coronado, L. L. Zhao, and G. C. Schatz. "The optical properties of metal nanoparticles: The influence of size, shape, and dielectric environment". *J. Phys. Chem. B*, 107:668, 2003.

[79] H. Kuwata, H. Tamaru, K. Esumi, and K. Miyano. "Resonant light scattering from metal nanoparticles: Practical analysis beyond Rayleigh approximation". *Appl. Phys. Lett.*, 83:4625, 2003.

[80] T. K. Sau, A. L. Rogach, F. Jäckel, T. A. Klar, and J. Feldmann. "Properties and applications of colloidal nonspherical noble metal nanoparticles". *Adv. Mater*., 22:1805, 2010.

[81] J. Ye, P. Van Dorpe, W. Van Roy, K. Lodewijks, I. De Vlaminck, G. Maes, and G. Borghs. "Fabrication and optical properties of gold semishells". *J. Phys. Chem. C*, 113:3110, 2009.

[82] U. Kreibig and M. Vollmer. "Optical properties of metal clusters". *Springer: Berlin*, 1995.

[83] K. Tanabe. "Field enhancement around metal nanoparticles and nanoshells: A systematic investigation". *J. Phys. Chem*. C, 112:15721, 2008.

[84] B. P. Rand, P. Peumans, and S. R. Forrest. "Long-range absorption enhancement in organic tandem thin-film solar cells containing silver nanoclusters". *J. Appl. Phys*., 96:7519, 2004.

[85] A. P. Kulkarni, K. M. Noone, K. Munechika, S. R. Guyer, and D. S. Ginger. "Plasmon-enhanced charge carrier generation in organic photovoltaic films using silver nanoprisms". *Nano Lett.*, 10:1501, 2010.

[86] H. Shen, P. Bienstman, and B. Maes. "Plasmonic absorption enhancement in organic solar cells with thin active layers". *J. Appl. Phys*., 106:073109, 2009.

[87] J. B. Khurgin and G. Sun. "Enhancement of optical properties of nanoscaled objects by metal nanoparticles". *J. Opt. Soc*. Am. B, 26:B83, 2009.

[88] R. Bardhan, N. K. Grady, J. R. Cole, A. Joshi, and N. J. Halas. "Fluorescence enhancement by au nanostructures: nanoshells and nanorods". *ACS Nano*, 3:744, 2009.

[89] A. Kinkhabwala, Z. Yu, S. Fan, Y. Avlasevich, K. Müllen, and W. E. Moerner. "Large single-molecule fluorescence enhancements produced by a bowtie nanoantenna". *Nature Photon*, 3:654, 2009.

[90] M. H. Chowdhury, S. Chakraborty, J. R. Lakowicz, and K. Ray. "Feasibility of using bimetallic plasmonic nanostructures to enhance the intrinsic emission of biomolecules". *J. Phys. Chem. C*, 115:16879, 2011.

[91] [86] T. Härtling, P. Reichenbach, and L. M. Eng. "Near-field coupling of a single fluorescent molecule and a spherical gold nanoparticle". *Opt. Express*, 15:12806, 2007.

[92] J. Kim, G. Dantelle, A. Revaux, M. Berard, A. Huignard, T. Gacoin, and J.-P. Boilot. "Plasmon-induced modification of fluorescent thin film emission nearby gold nanoparticle monolayers". *Langmuir*, 26:8842, 2010.

[93] S. Pan and L. J. Rothberg. "Enhancement of platinum octaethyl porphyrin phosphorescence near nanotextured silver surfaces". *J. Am. Chem. Soc*., 127:6087, 2005.

[94] E. Dulkeith, M. Ringler, T. A. Klar, J. Feldmann, A. Munoz Javier, and W. J. Parak. "Gold nanoparticles quench fluorescence by phase induced radiative rate suppression". *Nano Lett*., 5:585, 2005.

[95] R. Chhabra, J. Sharma, H. Wang, S. Zou, S. Lin, H. Yan, S. Lindsay, and Y. Liu. "Distance-dependent interactions between gold nanoparticles and fluorescent molecules with dna as tunable spacers". *Nanotechnology*, 20:485201, 2009.

[96] G. Schneider, G. Decher, N. Nerambourg, R. Praho, M. H. V. Werts, and M. Blanchard-Desce. "Distance-dependent fluorescence quenching on gold nanoparticles ensheathed with layer-by-layer assembled polyelectrolytes". *Nano Lett.*, 6:530, 2006.

[97] S. Kuhn, U. Hakanson, L. Rogobete, and V. Sandoghdar. "Enhancement of single-molecule fluorescence using a gold nanoparticle as an optical nanoantenna". *Phys. Rev. Lett*., 97:017402, 2006.

[98] K. Munechika, Y. Chen, A. F. Tillack, A. P. Kulkarni, I. Jen-La Plante, A. M. Munro, and D. S. Ginger. "Spectral control of plasmonic emission enhancement from quantum dots near single silver nanoprisms". *Nano Lett.,* 10:2598, 2010.

[99] F. Tam, G. P. Goodrich, B. R. Johnson, and N. J. Halas. "Plasmonic enhancement of molecular fluorescence". *Nano Lett*., 7:496, 2007.

[100] P. Bharadwaj and L. Novotny. "Spectral dependence of single molecule fluorescence enhancement". *Opt. Express*, 15:14266, 2007.

[101] Y. Chen, K. Munechika, and D. S. Ginger. "Dependence of fluorescence intensity on the spectral overlap between fluorophores and plasmon resonant single silver nanoparticles". *Nano Lett*., 7:690, 2007.

[102] Y. Chen, K. Munechika, I. Jen-La Plante, A. M. Munro, S. E. Skrabalak, Y. Xia, and D. S. Ginger. Excitation enhancement of CdSe quantum dots by single metal nanoparticles. Appl. Phys. Lett., 93:053106, 2008.

[103] V. Giannini, A. I. Fernandez-Dominguez, S. C. Heck, and S. A. Maier. "Plasmonic nanoantennas: Fundamentals and their use in controlling the radiative properties of nanoemitters". *Chem. Rev*., 111:3888, 2011.

[104] J. B. Khurgin and G. Sun. "Enhancement of optical properties of nanoscaled objects by metal nanoparticles". *J. Opt. Soc. Am. B*, 26:B83, 2009.

[105] Y. Cheng, T. Stakenborg, P. Van Dorpe, L. Lagae, M. Wang, H. Chen, and G. Borghs. "Fluorescence near gold nanoparticles for DNA sensing". *Anal. Chem*., 83:1307, 2011.

[106] E. Fort and S. Gresillon. "Surface enhanced fluorescence". *J. Phys. D: Appl. Phys*., 41:013001, 2008.

[107] M. Thomas, J.-J. Greffet, R. Carminati, and J. R. Arias-Gonzalez. "Singlemolecule spontaneous emission close to absorbing nanostructures". *Appl. Phys. Lett*., 85:3863, 2004.

[108] O. L. Muskens, V. Giannini, J. A. Sanchez-Gil, and J. Gomez Rivas. "Strong enhancement of the radiative decay rate of emitters by single plasmonic nanoantennas". *Nano Lett*., 7:2871, 2007.

[109] S. Pillai, K. R. Catchpole, T. Trupke, and M. A. Green. "Surface plasmon enhanced silicon solar cells". *Journal of Applied Physics*, 101(9), 2007.

[110] K. Nakayama, K. Tanabe, and H. A. Atwater. "Plasmonic nanoparticle enhanced light absorption in GaAs solar cells". *Applied Physics Letters*, 93(12), 2008.

[111] B. P. Rand, P. Peumans, and S. R. Forrest. "Long-range absorption enhancement in organic tandem thin-film solar cells containing silver nanoclusters". *Journal of Applied Physics*, 96(12):7519-7526, 2004

[112] P. N. Saeta, V. E. Ferry, D. Pacifici, J. N. Munday, and H. A. Atwater. "How much can guided modes enhance absorption in thin solar cells?" *Optics Express*, 17(23):20975-20990, 2009.

[113] H. R. Stuart and D. G. Hall. "Island size effects in nanoparticle-enhanced photodetectors". *Applied Physics Letters*, 73(26):3815-3817, 1998.

[114] V. E. Ferry, L. A. Sweatlock, D. Paciffci, and H. A. Atwater. "Plasmonic Nanostructure Design for Efficient Light Coupling into Solar Cells". *Nano Letters*, 8 (12):4391-4397, 2008.

[115] R. A. Pala, J. White, E. Barnard, J. Liu, and M. L. Brongersma. "Design of Plasmonic Thin-Film Solar Cells with Broadband Absorption Enhancements". *Advanced Materials*, 21(34):3504+, 2009.

[116] K. R. Catchpole and A. Polman. "Design principles for particle plasmon enhanced solar cells". *Applied Physics Letters*, 93(19), 2008.

[117] H. C. van de Hulst, "Light Scattering by Small Particles" (*Dover*, 1981).

[118] B. T. Draine, "The discrete dipole approximation and its application to interstellar graphite grains," *Astrophys. J.* 333, 848–872 (1988).

[119] S. Albaladejo, R. G´omez-Medina, L. S. Froufe-P´erez, H. Marinchio, R. Carminati, J. F. Torrado, G. Armelles, A. Garc´ıa-Mart´ın, and J. J. S´aenz, "Radiative corrections to the polarizability tensor of an electrically small anisotropic dielectric particle," *Opt. Express* 18, 3556–3567 (2010).

[120] M. Nieto-Vesperinas, J. J. S´aenz, R. G´omez-Medina, and L. Chantada, "Optical forces on small magnetodielectric magnetic particles," *Opt. Express* 18, 11428–11443 (2010).

[121] Deckman, H., C. Roxlo, and E. Yablonovitch, "Maximum statistical increase of optical absorption in textured semiconductor films". *Optics letters*, 1983. 8(9): p. 491-493.

[122] Green, M.A., "Solar cells: operating principles, technology, and system applications". 1982.

[123] Yablonovitch, E. and G.D. Cody, "Intensity enhancement in textured optical sheets for solar cells". *IEEE Transactions on Electron Devices*, 1982. 29(2): p. 300-305.

[124] Nakayama, K., K. Tanabe, and H.A. Atwater, "Plasmonic nanoparticle enhanced light absorption in GaAs solar cells". *Applied Physics Letters*, 2008. 93(12): p. 121904.

[125] Pillai, S., et al., "Surface plasmon enhanced silicon solar cells". *Journal of applied physics*, 2007. 101(9): p. 093105.

[126] Rand, B.P., P. Peumans, and S.R. Forrest, "Long-range absorption enhancement in organic tandem thin-film solar cells containing silver nanoclusters". *Journal of Applied Physics*, 2004. 96(12): p. 7519-7526.

[127] Schaadt, D., B. Feng, and E. Yu, "Enhanced semiconductor optical absorption via surface plasmon excitation in metal nanoparticles". *Applied Physics Letters*, 2005. 86(6): p. 063106.

[128] Stuart, H.R. and D.G. Hall, "Absorption enhancement in silicon-on-insulator waveguides using metal island films". *Applied Physics Letters*, 1996. 69(16): p. 2327-2329.

[129] Stuart, H.R. and D.G. Hall, "Island size effects in nanoparticle-enhanced photodetectors". *Applied Physics Letters*, 1998. 73(26): p. 3815-3817.

[130] Atwater, H.A. and A. Polman, "Plasmonics for improved photovoltaic devices". *Nature materials*, 2010. 9(3): p. 205-213.

[131] Bohren, C.F. and D.R. Huffman, "Absorption and scattering of light by small particles". 2008: John Wiley & Sons.

[132] Repän, T., et al., "Increased efficiency inside the CdTe solar cell absorber caused by plasmonic metal nanoparticles". *Energy Procedia*, 2014. 44: p. 229-233.

[133] Rakić, A.D., et al., "Optical properties of metallic films for vertical-cavity optoelectronic devices". *Applied optics*, 1998. 37(22): p. 5271-5283.

[134] Rakić, A.D., "Algorithm for the determination of intrinsic optical constants of metal films: application to aluminum". *Applied optics*, 1995. 34(22): p. 4755-4767.

[135] Aspnes, D. and A. Studna, "Dielectric functions and optical parameters of si, ge, gap, gaas, gasb, inp, inas, and insb from 1.5 to 6.0 ev". *Physical Review B*, 1983. 27(2): p. 985.

[136] E. Palik, "Handbook of Optical Constants of Solids", *Volumes I, II, and III, Academic Press Handbook Series, Elsevier Science & Tech*, 1985.

[137] A. D. Raki´c, "Algorithm for the determination of intrinsic optical constants of metal films: application to aluminum", *Appl. Opt.* 34 (22) (1995) 4755–4767.

[138] S. Tutihasi, G. G. Roberts, R. C. Keezer, R. E. Drews, "Optical properties of tellurium in the fundamental absorption region", *Phys. Rev*. 177 (1969) 1143–1150.

[139] Y. A. Akimov, W. S. Koh, "Resonant and nonresonant plasmonic nanoparticle enhancement for thin-film silicon solar cells". *Nanotechnology* 21 (23) (2010) 235201.

[140] Bailie, C.D., et al., "Semi-transparent perovskite solar cells for tandems with silicon and CIGS". *Energy & Environmental Science*, 2015. 8(3): p. 956-963.

[141] Boudreault, P.-L.T., A. Najari, and M. Leclerc, "Processable low-bandgap polymers for photovoltaic applications". *Chemistry of Materials*, 2010. 23(3): p. 456-469.

[142] Kojima, A., et al., "Organometal halide perovskites as visible-light sensitizers for photovoltaic cells". *Journal of the American Chemical Society*, 2009. 131(17): p. 6050-6051.

[143] Ball, J.M., et al., "Low-temperature processed meso-superstructured to thin-film perovskite solar cells". *Energy & Environmental Science*, 2013. 6(6): p. 1739-1743.

[144] Eperon, G.E., et al., "Formamidinium lead trihalide: a broadly tunable perovskite for efficient planar heterojunction solar cells". *Energy & Environmental Science*, 2014. 7(3): p. 982-988.

[145] Zhang, W., et al., "Enhancement of perovskite-based solar cells employing core–shell metal nanoparticles". *Nano letters*, 2013. 13(9): p. 4505-4510.

[146] Standridge, S.D., G.C. Schatz, and J.T. Hupp, "Distance dependence of plasmon-enhanced photocurrent in dye-sensitized solar cells". *Journal of the American Chemical Society*, 2009. 131(24): p. 8407-8409.

[147] Yang, J., Jingbi You, Chun-Chao Chen, Wan-Ching Hsu, Hai-ren Tan, Xing Wang Zhang, Ziruo Hong, and Yang Yang. "Plasmonic polymer tandem solar cell". *ACS Nano*, 2011. 5(8): p. 6210-6217.

[148] Catchpole, K. and A. Polman, 'Plasmonic solar cells". *Optics express*, 2008. 16(26): p. 21793-21800.

[149] Reineck, P., et al., "A Solid-State Plasmonic Solar Cell via Metal Nanoparticle Self-Assembly". *Advanced Materials*, 2012. 24(35): p. 4750-4755.

[150] Atwater, H.A. and A. Polman, "Plasmonics for improved photovoltaic devices". *Nature materials*, 2010. 9(3): p. 205-213.

[151] Repän, T., et al., "Increased efficiency inside the CdTe solar cell absorber caused by plasmonic metal nanoparticles". *Energy Procedia*, 2014. 44: p. 229-233.

[152] Baikie, Baikie, Tom, et al. "Synthesis and crystal chemistry of the hybrid perovskite (CH 3 NH 3) PbI 3 for solid-state sensitised solar cell applications." *Journal of Materials Chemistry* A 1.18 (2013): 5628-5641.

[153] Rakić, A.D., et al., "Optical properties of metallic films for vertical-cavity optoelectronic devices". *Applied optics*, 1998. 37(22): p. 5271-5283.

[154] Phillips, L.J., et al., "Dispersion relation data for methylammonium lead triiodide perovskite deposited on a (100) silicon wafer using a two-step vapour-phase reaction process". *Data in brief*, 2015. 5: p. 926-928.

[155] Bohren, C.F. and D.R. Huffman, "Absorption and scattering of light by small particles". *John Wiley & Sons*. 2008